Chapter

# Metal- and Dielectric-Loaded Waveguide: An Artificial Material for Tailoring the Waveguide Propagation Characteristics

*Vishal Kesari*

## Abstract

In the present chapter a number of loaded structures are studied with circular cross-section to explore the deviation in their dispersion characteristics from their parent circular waveguide. The dielectric and/or metal loading to the waveguide tailors its dispersion characteristics. In general, the dielectric depresses and the metal elevates the dispersion characteristics from the characteristics of their parent circular waveguide. The axial periodicity results in periodic dispersion characteristics with a lower and an upper cut-off frequency (bandpass). However such a characteristic is not reported for the azimuthal periodic structures. The bandpass characteristic arises due to the shaping of the dispersion characteristics. Therefore the dispersion shaping is only possible with axial periodicity and not with the azimuthal periodicity. The sensitivity of the structure (geometry) parameters on the lower and upper cut-off frequencies, the extent of passband and the dispersion shaping are also included. In the axial periodic structures, the periodicity is found to be the most sensitive parameter for tailoring the dispersion characteristics and the disc-hole radius is the most sensitive parameter for shifting the dispersion characteristics over the frequency axis.

**Keywords:** periodically loaded waveguide, metal and dielectric loading, disc-loaded circular waveguide, dispersion characteristics, dispersion shaping

## 1. Introduction

Waveguides, due to their low insertion loss and high power handling capabilities at microwave and millimeter-wave frequencies, are the transmission line commonly used for transmitting or propagating or guiding the signals of these frequencies from one point to another. The propagation characteristics of a guiding structure are generally represented by its dispersion characteristics. The dispersion characteristics are the study of structure supported frequency for a given phase propagation constant, and most commonly being plotted as the supported angular frequency $\omega$ ($= 2\pi f$, $f$ being frequency) against the phase propagation constant $\beta$. Therefore, the dispersion characteristics are also known as $\omega - \beta$ characteristics. The dispersion ($\omega - \beta$) characteristics of a waveguide is a hyperbola that has a cutoff frequency, more specifically a lower cutoff frequency. All the signals having

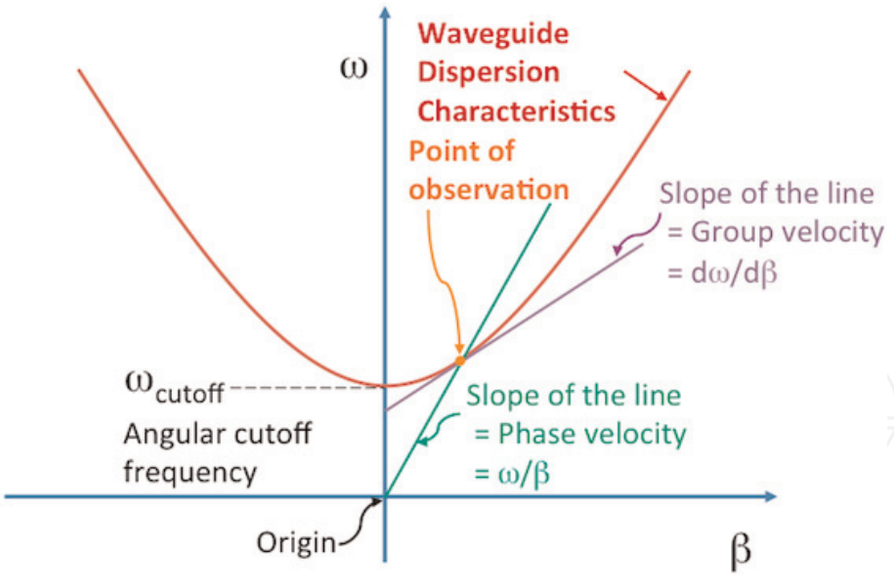


**Figure 1.**
*$\omega - \beta$ dispersion characteristics of a circular waveguide showing the waveguide cutoff frequency and phase and group velocities.*

frequencies above this lower cutoff frequency are allowed to propagate through the waveguide, and the signals having frequencies below this frequency will face a high reflection. Because of this characteristics a waveguide is inherently a high pass filter. The waveguide supports two kinds of velocities namely the phase velocity and the group velocity. The phase velocity at a chosen frequency is the one with which the signal of constant phase travels, which is represented by the slope of a line joining a chosen frequency point on $\omega - \beta$ dispersion characteristics to the origin (point representing zero frequency and zero phase propagation constant), i.e. mathematically given as $\omega/\beta$. The group velocity at a chosen frequency point is the one with which the energy in signal travels, which is represented by the slope of the $\omega - \beta$ dispersion characteristics at the chosen frequency point, i.e. mathematically given as $d\omega/d\beta$ (**Figure 1**). Thus, one can control the supported phase and group velocities in a waveguide by tailoring its dispersion characteristics. Such tailoring can be achieved by loading the waveguide by metal and/ or dielectric in to the smooth wall waveguide [1–5]. The characteristics (propagation or dispersion) of the conventional (smooth wall) waveguide changes with the metal and/or dielectric loading, and the same cannot be generated naturally. Therefore, the metal- and/or dielectric-loaded waveguide may be considered as artificially created material or artificial material. In part of the chapter to follow, a number of circular waveguide models containing various metal and/or dielectric loading are considered (Section 2). The electromagnetic boundary conditions (Section 3) and the dispersion relations (Section 4) of these loaded waveguides are outlined. Further, the dispersion characteristics of all the considered loaded waveguides are discussed with their sensitivity against variation in structure (geometrical) parameters (Section 5). Finally, the conclusion is drawn (Section 6).

## 2. Structure models

Although, the considered structures being a single conductor structure support TE ($E_z = 0$) as well as TM ($H_z = 0$) modes, they are being analyzed for the TE modes. The structures excited in these modes are of the interest for a specific class of vacuum electronic fast-wave devices, specifically the gyro-devices. In the

category of gyro-devices, for the broadband amplifier namely the gyro-traveling-wave tube (gyro-TWT) the growth rate of the TM-mode vanishes at higher frequencies [6]. The models are also restricted to circular waveguide and the analyses are carried out in cylindrical $(r, \theta, z)$ system of coordinates.

## 2.1 Dielectric-loaded circular waveguide

In this section, we will explore two variants of dielectric-loaded structure: (i) the circular waveguide with dielectric lining on metal wall (**Figure 2**), and (ii) the circular waveguide with dielectric coaxial insert (**Figure 3**) for their dispersion characteristics and the tailoring of these characteristics with change of the relative permittivity of the dielectric material.

### *2.1.1 Circular waveguide with dielectric lining on metal wall*

This model (model-1) includes a metallic circular waveguide of inner radius $r_W$, inner wall of which is containing a dielectric lining of inner radius $r_L$ and relative permittivity $\varepsilon_r$ for the full length of the waveguide [7]. (Here, the waveguide is considered to be infinitely long and there is no reflection of the traveling signals

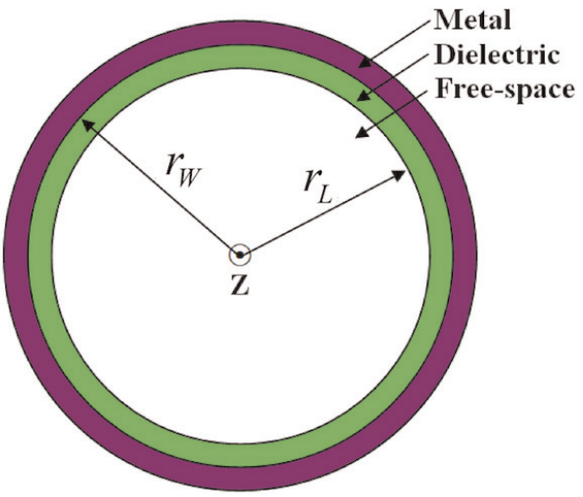


**Figure 2.**
*Circular waveguide with dielectric lining on metal wall [7].*

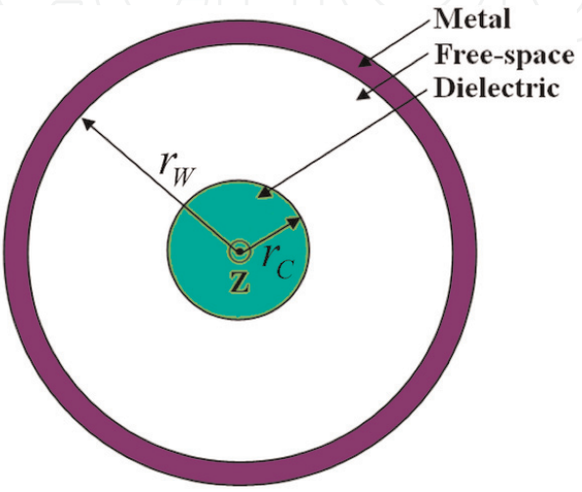


**Figure 3.**
*Circular waveguide with dielectric coaxial insert [7].*

from the waveguide extremes). Thus the radial thickness of the dielectric lining can be calculated as $r_W - r_L$. For the sake of analysis, the structure may be divided into two analytical regions, the central free-space (dielectric free) region I: $0 \le r < r_L$, $0 \le z < \infty$; and the dielectric filled region II: $r_L \le r < r_W$, $0 \le z < \infty$ (**Figure 2**). The relevant (axial magnetic and azimuthal electric) field intensity components may be written as [7]:

In region I:

$$H_z^I = \sum_{n=-\infty}^{+\infty} A_n^I J_0\{\gamma_n^I r\} \exp j(\omega t - \beta_n z) \tag{1}$$

$$E_\theta^I = j\omega\mu_0 \sum_{n=-\infty}^{+\infty} \frac{1}{\gamma_n^I} A_n^I J_0'\{\gamma_n^I r\} \exp j(\omega t - \beta_n z) \tag{2}$$

In region II:

$$H_z^{II} = \sum_{n=-\infty}^{+\infty} \left(A_n^{II} J_0\{\gamma_n^{II} r\} + B_n^{II} Y_0\{\gamma_n^{II} r\}\right) \exp j(\omega t - \beta_n z) \tag{3}$$

$$E_\theta^{II} = j\omega\mu_0 \sum_{n=-\infty}^{+\infty} \frac{1}{\gamma_n^{II}} \left(A_n^{II} J_0'\{\gamma_n^{II} r\} + B_n^{II} Y_0'\{\gamma_n^{II} r\}\right) \exp j(\omega t - \beta_n z) \tag{4}$$

where $J_0$ and $Y_0$ are the zeroth-order Bessel functions of the first and second kinds, respectively. Prime with a function represents the derivative with respect to its argument. $A_n^I$, $A_n^{II}$ and $B_n^{II}$ are the field constants, superscript identifying its value, in different analytical regions. $\gamma_n^I \left[= \left(k^2 - \beta_n^2\right)^{1/2}\right]$ and $\gamma_n^{II} \left[= \left(\varepsilon_r k^2 - \beta_n^2\right)^{1/2}\right]$ are the radial propagation constants in regions I and II, respectively. $\beta_n$ and $k$ are the phase and the free-space propagation constants, respectively [7].

### *2.1.2 Circular waveguide with dielectric coaxial insert*

Similar to model-1, this model (model-2) also contains a metallic circular waveguide of inner radius $r_W$, inner wall of which is free from any dielectric. The model includes a coaxial dielectric insert of radius $r_C$ and relative permittivity $\varepsilon_r$ for the full length of the waveguide (**Figure 3**) [7].

For the sake of analysis, the structure may be divided into two analytical regions, the central dielectric filled region I: $0 \le r < r_C$, $0 \le z < \infty$; and the free-space (dielectric free) region II: $r_C \le r < r_W$, $0 \le z < \infty$. The relevant (axial magnetic and azimuthal electric) field intensity components may be written same as for model-1 (1)–(4), in which the radial propagation constants $\gamma_n^I$ and $\gamma_n^{II}$ are interpreted as: $\gamma_n^I = \left(\varepsilon_r k^2 - \beta_n^2\right)^{1/2}$ and $\gamma_n^{II} = \left(k^2 - \beta_n^2\right)^{1/2}$, respectively [7].

## 2.2 Metal-loaded circular waveguide

In Section 2.1, we have studied the dispersion characteristics of dielectric-loaded structures. In the present section, we will explore three variants of all metal-loaded structure: (i) the conventional annular metal disc-loaded circular waveguide (**Figure 4**), (ii) the interwoven-disc-loaded circular waveguide (**Figure 5**), and (iii) metal vane-loaded circular waveguide (**Figure 6**) for their dispersion characteristics and the effect of change of the geometry parameters on these characteristics.

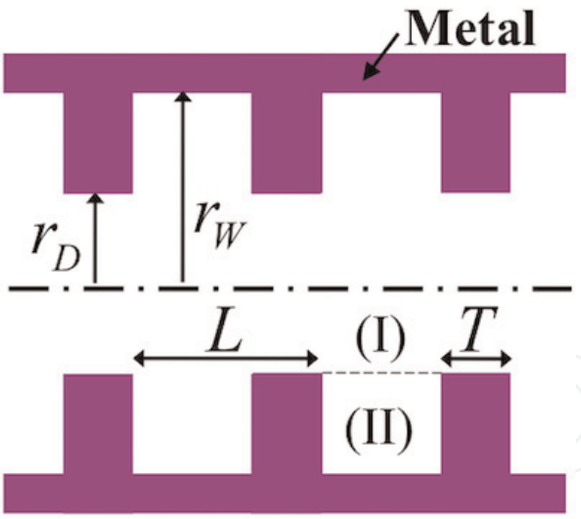


**Figure 4.**
*Circular waveguide with annular metal discs [9–13].*

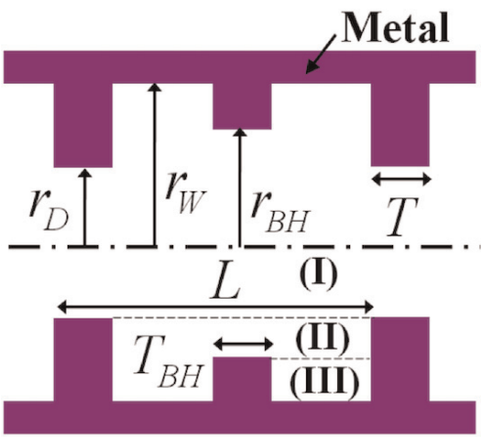


**Figure 5.**
*Interwoven disc-loaded circular waveguides [2, 9, 14, 15].*

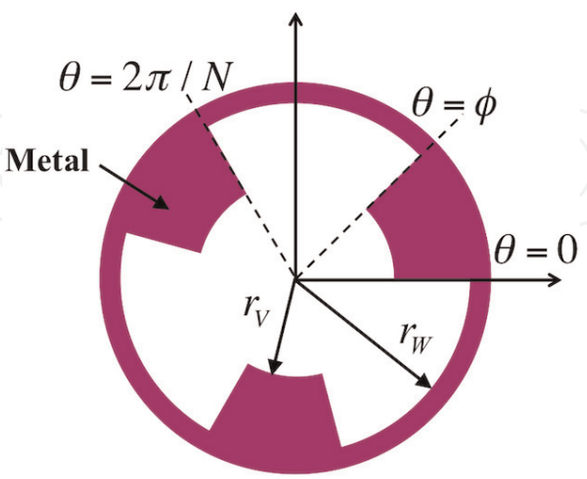


**Figure 6.**
*Circular waveguide loaded with metal vanes [16–18].*

### *2.2.1 Circular waveguide with annular metal discs*

In this model (model-3) a circular metallic waveguide of inner radius $r_W$ is considered in which annular disc of thickness $T$, inner radius $r_D$ and outer radius $r_W$

are arranged periodically with periodicity $L$. The structure is commonly known as the disc-loaded circular waveguide (conventional) (**Figure 4**) [2, 5, 8–13]. As the structure is periodic, therefore one period of the structure coupled with Floquet's theorem is sufficient for the analysis of the infinitely long structure [1, 2, 5, 8, 9]. For the sake of analysis, the structure may be divided into two analytical regions, the central free-space (disc free) region I: $0 \le r < r_D$, $0 \le z < \infty$; and the disc occupied region II: $r_D \le r < r_W$, $0 \le z \le L - T$ (**Figure 4**). The disc free and disc occupied regions are assumed to support propagating (traveling) and stationary waves, respectively. The relevant (axial magnetic and azimuthal electric) field intensity components in the region I is given by (1) and (2) and in the region II may be written as [2, 5, 9–13]:

In region II:

$$H_z^{II} = \sum_{m=1}^{\infty} A_m^{II} Z_0\{\gamma_m^{II} r\} \exp(j\omega t) \sin(\beta_m z) \tag{5}$$

$$E_\theta^{II} = j\omega\mu_0 \sum_{m=1}^{\infty} \frac{1}{\gamma_m^{II}} A_m^{II} Z_0'\{\gamma_m^{II} r\} \exp(j\omega t) \sin(\beta_m z) \tag{6}$$

where $Z_0\{\gamma_m^{II} r\} = J_0\{\gamma_m^{II} r\} Y_0'\{\gamma_m^{II} r_W\} - J_0'\{\gamma_m^{II} r_W\} Y_0\{\gamma_m^{II} r\}$; $A_m^{II}$ is the field constants, superscript identifying its value, in different analytical regions.

$\gamma_m^{II} \left[= \left(k^2 - \beta_m^2\right)^{1/2}\right]$ is the radial propagation constant in region II. $\beta_n$, defined as $\beta_n = \beta_0 + 2\pi n/L$, is the axial phase propagation constant in region I with $\beta_0$ as the axial phase propagation constant for fundamental space harmonic, and $n$ [= 0, ±1, ±2, ±3, ...] as space harmonic number. $\beta_m$, defined as $\beta_m = m\pi/(L - T)$, is the axial propagation constants in region II with $m$ (= 1, 2, 3, ...) as the modal harmonic numbers in region II [2, 5, 9–13].

### *2.2.2 Interwoven-disc-loaded circular waveguide*

This model (model-4) differs from the conventional disc-loaded circular waveguide due to different additional disc included in between two identical consecutive discs of conventional disc-loaded circular waveguide [2, 9, 14, 15]. Thus, this model is considered with a circular metallic waveguide of inner radius $r_W$ in which annular disc of thickness $T$, inner radius $r_D$ and outer radius $r_W$ are arranged periodically with periodicity $L$. In addition, another annular disc of thickness $T_{BH}$, inner radius $r_{BH}$ and outer radius $r_W$ are also arranged periodically with periodicity $L$ such that the disc of thickness $T_{BH}$ is placed in middle of two identical consecutive discs of thickness $T$. The structure is known as the interwoven-disc-loaded circular waveguide. Similar to conventional disc-loaded circular waveguide, this structure is also periodic, therefore considering unit cell of the structure with Floquet's theorem suffices for the analysis of the infinitely long structure. The analytical regions of the model may be considered as: (i) region I: $0 \le r < r_D$, $0 \le z < \infty$; (ii) region II: $r_D \le r < r_{BH}$, $0 \le z \le L - T$; and (iii) region III: $r_{BH} \le r < r_W$, $0 \le z \le (L - T - T_{BH})/2$, where $L - T$ and $(L - T - T_{BH})/2$ represent the axial-gaps between two consecutive discs of smaller hole and between discs of bigger and smaller holes (**Figure 5**).

Similar to the conventional disc-loaded circular waveguide (model-3), it is assumed that the disc free (I) and disc occupied (II and III) regions, respectively, support propagating and standing waves. The relevant (axial magnetic and azimuthal electric) field intensity components in the region I is given by (1) and (2) and in the regions II and III may be written as [2, 9, 14, 15]:

In region II:

$$H_z^{II} = \sum_{m=1}^{\infty} \left[A_m^{II} J_0\{\gamma_m^{II} r\} + B_m^{II} Y_0\{\gamma_m^{II} r\}\right] \exp(j\omega t) \sin(\beta_m z) \tag{7}$$

$$E_\theta^{II} = j\omega\mu_0 \sum_{m=1}^{\infty} \frac{1}{\gamma_m^{II}} \left[A_m^{II} J_0'\{\gamma_m^{II} r\} + B_m^{II} Y_0'\{\gamma_m^{II} r\}\right] \exp(j\omega t) \sin(\beta_m z) \tag{8}$$

In region III:

$$H_z^{III} = \sum_{p=1}^{\infty} A_p^{III} Z_0\left\{\gamma_p^{III} r\right\} \exp(j\omega t) \sin\left(\beta_p z\right) \tag{9}$$

$$E_\theta^{III} = j\omega\mu_0 \sum_{p=1}^{\infty} \frac{1}{\gamma_p^{III}} A_p^{III} Z_0'\{\gamma_m^{III} r\} \exp(j\omega t) \sin\left(\beta_p z\right), \tag{10}$$

where $Z_0\left\{\gamma_p^{III} r\right\} = J_0\left\{\gamma_p^{III} r\right\} Y_0'\left\{\gamma_p^{III} r_W\right\} - J_0'\left\{\gamma_p^{III} r_W\right\} Y_0\left\{\gamma_p^{III} r\right\}$; $A_m^{II}$, $B_m^{II}$ and $A_p^{III}$ are the field constants, superscript identifying its value, in different analytical regions. $\gamma_m^{II}\left[= \left(k^2 - \beta_m^2\right)^{1/2}\right]$ and $\gamma_p^{III}\left[= \left(k^2 - \beta_p^2\right)^{1/2}\right]$ are the radial propagation constants in regions II and III, respectively. The axial phase propagation constants $\beta_n$ in region I and $\beta_m$ in region II are defined in the same manner as for model-3. $\beta_p$ $[= 2p\pi/(L - T - T_{BH})]$ is the axial phase propagation constants in region III; here $p$ is the modal harmonic number in region III [2, 9, 14, 15].

### *2.2.3 Circular waveguide loaded with metal vanes*

This model (model-5) considers a circular waveguide of radius $r_W$ and $N$ number of metal vanes of vane-inner-tip radius $r_V$ and vane angle $\phi$ extending axially over the length of the waveguide arranged on the waveguide wall to maintain the azimuthal periodicity (**Figure 6**) [16–18]. Clearly, the azimuthal periodicity is $2\pi/N$. For the analysis of the structure, it may be divided into two regions; (i) the central cylindrical vane-free free-space region I: $0 \le r < r_V$, $0 \le \theta < 2\pi$, and (ii) the free-space region II between two consecutive metal vanes $r_V \le r \le r_W$, $\phi < \theta < 2\pi/N$(**Figure 6**). The relevant (axial magnetic and azimuthal electric) field intensity components in the regions I and II may be written as [16–18]:

In region I:

$$H_z^I = \sum_{q=-\infty}^{+\infty} A_q^I J_q\{\gamma^I r\} \exp(-jq\theta) \tag{11}$$

$$E_\theta^I = \frac{j\omega\mu_0}{\gamma^I} \sum_{q=-\infty}^{+\infty} A_q^I J_q'\{\gamma^I r\} \exp(-jq\theta) \tag{12}$$

In region II:

$$H_z^{II} = \sum_{v=0}^{+\infty} \left[A_v^{II} J_v\{\gamma^{II} r\} + B_v^{II} Y_v\{\gamma^{II} r\}\right] \cos\left(\frac{v\pi(\theta - \phi)}{2\pi/N - \phi}\right) \tag{13}$$

$$E_\theta^{II} = \frac{j\omega\mu_0}{\gamma^{II}} \sum_{v=0}^{+\infty} \left[A_v^{II} J_v'\{\gamma^{II} r\} + B_v^{II} Y_v'\{\gamma^{II} r\}\right] \cos\left(\frac{v\pi(\theta - \phi)}{2\pi/N - \phi}\right) \tag{14}$$

where $A_q^I$, $A_v^{II}$ and $B_v^{II}$ are the field constants; $J$ and $Y$ are the ordinary Bessel function of first and second kinds, respectively, with their primes representing the

derivatives with respect to their arguments. $q$ is an integer; and $v$ is a non-negative integer. $\gamma^I = \gamma^{II}\left(= \left(k^2 - \beta^2\right)^{1/2}\right)$ and $\beta$ are the radial and the axial phase propagation constants, respectively. In order to include the effect of azimuthal harmonics due to angular periodicity of the structure, the azimuthal dependence is considered as $\exp(-jv\theta)$, such that $v = s + qN$, where $s$ is also an integer [16–18].

### 2.3 Metal- and dielectric-loaded circular waveguide

In Sections 2.1 and 2.2, we have respectively explored the independent dielectric- and metal-loaded structures. However, in this section we will study the metal as well as dielectric loading in the circular waveguide.

#### *2.3.1 Circular waveguide loaded with dielectric and metal discs*

This model (model-6) is formed by alternatively stacking the metal and dielectric discs each of same disc hole radii $r_D$. This is similar to conventional disc-loaded circular waveguide in which the volume between two consecutive metal discs is filled with dielectric of relative permittivity $\varepsilon_r$. Similar to conventional disc-loaded circular waveguide for the sake of analysis, one may divide the structure into two regions: central disc free region I: $0 \le r < r_D$, $0 < z < \infty$, and disc occupied region II: $r_D \le r < r_W$, $0 < z < L - T$ (**Figure 7**). The relevant (axial magnetic and azimuthal electric) field intensity components in the regions I and II may be given by (1), (2), (5) and (6). In (5) and (6), the radial propagation constant in region II is interpreted as $\gamma_m^{II} = \left(\varepsilon_r k^2 - \beta_m^2\right)^{1/2}$ [19].

#### *2.3.2 Circular waveguide loaded with dielectric and metal discs having different hole radius*

This model (model-7) is similar to that of model-6, which has a circular waveguide consisting of alternate dielectric and metal discs, such that the hole-radius of metal discs is lesser than that of dielectric discs [20]. For the purpose of analysis, one may divide the structure into three regions: i) the central disc free region I: $0 \le r < r_D$, $0 < z < \infty$; ii) the disc occupied free space region II: $r_D \le r < r_{DD}$, $0 < z < L - T$; and iii) the dielectric filled disc occupied region III: $r_{DD} \le r < r_W$, $0 < z < L - T$; where $r_{DD}$ is the hole radius of dielectric disc. It is considered that the region I (disc free region) supports propagating and regions II and III (disc occupied regions) support standing waves [20].

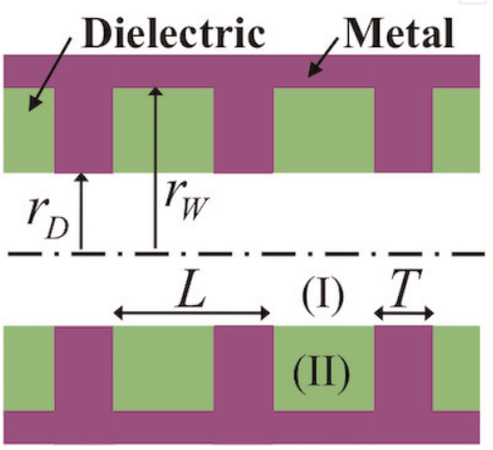


**Figure 7.**
*Circular waveguide loaded with dielectric and metal discs [19].*

The relevant (axial magnetic and azimuthal electric) field intensity components in the region I may be given by (1) and (2), and in regions II and III are written as [20]:

In region II:

$$H_z^{II} = \sum_{m=1}^{\infty} \left[A_m^{II} J_0\{\gamma_m^{II} r\} + B_m^{II} Y_0\{\gamma_m^{II} r\}\right] \exp(j\omega t) \sin(\beta_m z) \tag{15}$$

$$E_\theta^{II} = j\omega\mu_0 \sum_{m=1}^{\infty} \frac{1}{\gamma_m^{II}} \left[A_m^{II} J_0'\{\gamma_m^{II} r\} + B_m^{II} Y_0'\{\gamma_m^{II} r\}\right] \exp(j\omega t) \sin(\beta_m z) \tag{16}$$

In region III:

$$H_z^{III} = \sum_{m=1}^{\infty} A_m^{III} Z_0\{\gamma_m^{III} r\} \exp(j\omega t) \sin(\beta_m z) \tag{17}$$

$$E_\theta^{III} = j\omega\mu_0 \sum_{m=1}^{\infty} \frac{1}{\gamma_m^{III}} A_m^{III} Z_0'\{\gamma_m^{III} r\} \exp(j\omega t) \sin(\beta_m z) \tag{18}$$

where $Z_0\{\gamma_m^{III} r\} = J_0\{\gamma_m^{III} r\} Y_0'\{\gamma_m^{III} r_W\} - J_0'\{\gamma_m^{III} r_W\} Y_0\{\gamma_m^{III} r\}$; $A_m^{II}$, $B_m^{II}$ and $A_m^{III}$ are the field constants in different analytical regions, identified by given superscript, respectively. $\gamma_n^I \left[= \left(k^2 - \beta_n^2\right)^{1/2}\right]$, $\gamma_m^{II} \left[= \left(k^2 - \beta_m^2\right)^{1/2}\right]$, and $\gamma_m^{III} \left[= \left(\varepsilon_r k^2 - \beta_m^2\right)^{1/2}\right]$ are the radial propagation constants in regions I, II, and III, respectively (**Figure 8**). The axial phase propagation constants $\beta_n$ in region I and $\beta_m$ in regions II and III are defined in the same manner as for model-3 [20].

### *2.3.3 Circular waveguide loaded with alternate dielectric and metal vanes*

This model (model-8) is similar to model-5 except the region II filled with dielectric of relative permittivity $\varepsilon_r$ between the two consecutive metal vanes [21]. For the sake of analysis, the structure may be divided into two regions; (i) the central cylindrical vane-free free-space region I: $0 \le r < r_V$, $0 \le \theta < 2\pi$, and (ii) the dielectric filled region II between two consecutive metal vanes: $r_V \le r \le r_W$, $< \theta < 2\pi/N$ (**Figure 9**). The relevant (axial magnetic and azimuthal electric) field intensity components in the regions I and II may be given by (11)–(14), in which the radial propagation constant is given as: $\gamma^{II} = \left(\varepsilon_r k^2 - \beta^2\right)^{1/2}$ [21].

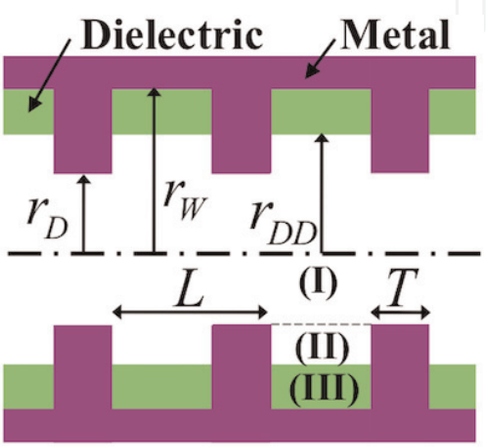


**Figure 8.**
*Circular waveguide loaded with dielectric and metal discs with the hole radius of metal discs lesser than that of dielectric discs [20].*

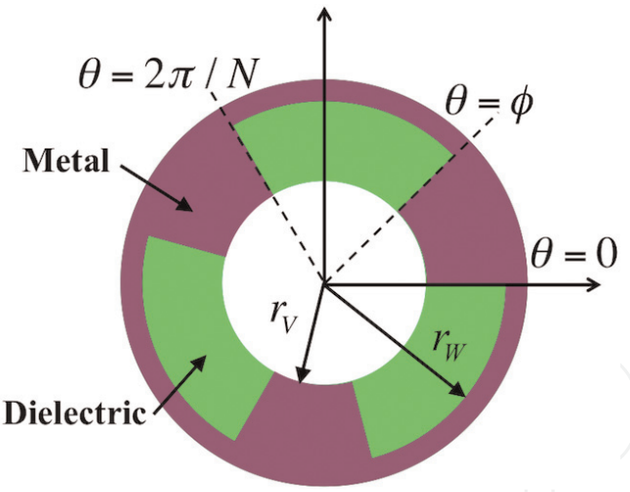


**Figure 9.**
*Circular waveguide loaded with alternate dielectric and metal vanes [21].*

## 3. Boundary conditions

One of the general boundary conditions comprising all the considered models is due to the null tangential electric field intensity at the inner surface of the metallic waveguide that is represented as [2, 5, 9–21]:

$$E_\theta = 0\big|_{r=r_W} \quad 0 < z < \infty \tag{19}$$

*Model-1:* The relevant electromagnetic boundary conditions for model-1 may be written in the mathematical form as [7]:

$$H_z^I = H_z^{II}\big|_{r=r_L} \quad 0 < z < \infty \tag{20}$$

$$E_\theta^I = E_\theta^{II}\big|_{r=r_L} \quad 0 < z < \infty \tag{21}$$

The boundary conditions (20) and (21) state the continuity of the axial component of magnetic and the azimuthal component of electric field intensities at the interface, $r = r_L$, between the regions I and II (**Figure 2**) [7].

*Model-2:* The relevant electromagnetic boundary conditions for model-2 (**Figure 3**) may be written in the mathematical form as [7]:

$$H_z^I = H_z^{II}, \quad 0 < z < \infty\big|_{r=r_C} \tag{22}$$

$$E_\theta^I = E_\theta^{II}, \quad 0 < z < \infty\big|_{r=r_C} \tag{23}$$

The boundary conditions (22) and (23) state the continuity of the axial component of magnetic and the azimuthal component of electric field intensities at the interface, $r = r_C$, between the regions I and II (**Figure 3**) [7].

*Model-3:* The relevant electromagnetic boundary conditions for model-3 (**Figure 4**) may be written in the mathematical form as [2, 5, 9–13]:

$$H_z^I = H_z^{II} \quad 0 < z < L - T\big|_{r=r_D} \tag{24}$$

$$E_\theta^I = \begin{cases} E_\theta^{II} & 0 < z < L - T \\ 0 & L - T \le z \le L \end{cases}\Bigg|_{r=r_D} \tag{25}$$

The boundary conditions (24) and (25) state the continuity of the axial component of magnetic and the azimuthal component of electric field intensities at the interface, $r = r_D$, between the regions I and II, and the null azimuthal component of electric field intensity at the disc hole metallic surface (**Figure 4**) [2, 5, 9–13].

*Model-4:* The boundary conditions (24) and (25) are also true for the model-4 (**Figure 5**) at the interface, $r = r_D$, between the regions I and II. The additional boundary conditions at the interface, $r = r_{BH}$, between the regions II and III may be written as [2, 9, 14, 15]:

$$H_z^{II} = H_z^{III} \quad 0 \le z \le (L - T - T_{BH})/2\big|_{r=r_{BH}} \tag{26}$$

$$E_\theta^{II} = \begin{cases} E_\theta^{III} & 0 \le z \le (L - T - T_{BH})/2 \\ 0 & (L - T - T_{BH})/2 \le z \le (L - T + T_{BH})/2 \end{cases}\Bigg|_{r=r_{BH}} \tag{27}$$

The boundary conditions (26) and (27) state the continuity of the axial component of magnetic and the azimuthal component of electric field intensities at the interface, $r = r_{BH}$, between the regions II and III, and the null azimuthal component of electric field intensity at the disc hole metallic surface (**Figure 5**) [2, 9, 14, 15].

*Model-5:* The relevant electromagnetic boundary conditions for model-5 (**Figure 6**) may be written in the mathematical form as [16–18]:

$$H_z^I = H_z^{II} \qquad \phi \le \theta \le 2\pi/N\big|_{r=r_V} \tag{28}$$

$$E_\theta^I = \begin{cases} 0 & 0 \le \theta < \phi \\ E_\theta^{II} & \phi \le \theta \le 2\pi/N \end{cases}\Bigg|_{r=r_V} \tag{29}$$

The boundary conditions (28) and (29) state the continuity of the axial component of magnetic and the azimuthal component of electric field intensities at the interface, $r = r_V$, between the regions I and II, and the null azimuthal component of electric field intensity at the vane tip metallic surface (**Figure 6**) [16–18].

*Model-6:* The relevant electromagnetic boundary conditions for model-6 (**Figure 7**) are given by (24) and (25), same as for model-3 (**Figure 4**) [19].

*Model-7:* The relevant electromagnetic boundary conditions (24) and (25) are also true for the model-7 (**Figure 8**) at the interface, $r = r_D$, between the regions I and II. The additional boundary conditions at the interface, $r = r_{DD}$, between the regions II and III may be written as [20]:

$$H_z^{II} = H_z^{III} \qquad 0 < z < L - T\big|_{r=r_{DD}} \tag{30}$$

$$E_\theta^{II} = E_\theta^{III} \qquad 0 < z < L - T\big|_{r=r_{DD}} \tag{31}$$

The boundary conditions (30) and (31), respectively, state the continuity of the axial magnetic and the azimuthal electric field intensities at the interface, $r = r_{DD}$, between the disc occupied free space region II and disc-occupied dielectric region III (**Figure 8**) [20].

*Model-8:* The relevant electromagnetic boundary conditions for model-8 (**Figure 9**) are given by (28) and (29), same as for model-5 (**Figure 6**) [21].

## 4. Dispersion relations

In general, the field intensity components (**1**)–(18) contain unknown field constants. In order to establish relations between these unknown field constants, the

relevant field intensity components are substituted into the respective boundary conditions. Further, the algebraic manipulations of the obtained relations between these field constants eliminate all the field constants, and it results in a characteristic relation of the model known as the dispersion relation. The dispersion relations of various considered models are:

Model-1 [7]:

$$\begin{aligned}&\gamma^{II}J_0'\{\gamma^I r_L\}\left(J_0\{\gamma^{II}r_L\}Y_0'\{\gamma^{II}r_W\}-Y_0\{\gamma^{II}r_L\}J_0'\{\gamma^{II}r_W\}\right)\\&-\gamma^I J_0\{\gamma^I r_L\}\left(J_0'\{\gamma^{II}r_L\}Y_0'\{\gamma^{II}r_W\}-Y_0'\{\gamma^{II}r_L\}J_0'\{\gamma^{II}r_W\}\right)=0\end{aligned} \tag{32}$$

Model-2 [7]:

$$\begin{aligned}&\gamma^{II}J_0'\{\gamma^I r_C\}\left(J_0\{\gamma^{II}r_C\}Y_0'\{\gamma^{II}r_W\}-Y_0\{\gamma^{II}r_C\}J_0'\{\gamma^{II}r_W\}\right)\\&-\gamma^I J_0\{\gamma^I r_C\}\left(J_0'\{\gamma^{II}r_C\}Y_0'\{\gamma^{II}r_W\}-Y_0'\{\gamma^{II}r_C\}J_0'\{\gamma^{II}r_W\}\right)=0\end{aligned} \tag{33}$$

Model-3 [2, 5, 9–13]:

$$\det\left|M_{nm}J_0\{\gamma_n^I r_D\}Z_0'\{\gamma_m^{II}r_D\}-Z_0\{\gamma_m^{II}r_D\}J_0'\{\gamma_n^I r_D\}\right|=0 \tag{34}$$

where

$$M_{nm}=\frac{\gamma_n^I\beta_m^{II}\left(1-(-1)^m\exp\left[-j\beta_n^I(L-T)\right]\right)}{\gamma_m^{II}\left[\beta_m^{II}-\exp\left(-j\beta_0^I L\right)\left(\beta_m^{II}\cos\left(\beta_m^{II}L\right)+j\beta_n^I\sin\left(\beta_m^{II}L\right)\right)\right]}. \tag{35}$$

Model-4 [2, 9, 14, 15]:

$$\det\left|M_{nm}J_0\{\gamma_n^I r_D\}\left[J_0'\{\gamma_m^{II}r_D\}+\xi Y_0'\{\gamma_m^{II}r_D\}\right]-J_0'\{\gamma_n^I r_D\}\left[J_0\{\gamma_m^{II}r_D\}+\xi Y_0\{\gamma_m^{II}r_D\}\right]\right|=0 \tag{36}$$

where

$$\xi=\frac{\gamma_p^{III}J_0'\{\gamma_m^{II}r_{BH}\}Z_0\{\gamma_m^{III}r_{BH}\}-\gamma_m^{II}J_0\{\gamma_m^{II}r_{BH}\}Z_0'\{\gamma_m^{III}r_{BH}\}}{\gamma_m^{II}Y_0\{\gamma_m^{II}r_{BH}\}Z_0'\{\gamma_m^{III}r_{BH}\}-\gamma_m^{III}Y_0'\{\gamma_m^{II}r_{BH}\}Z_0\{\gamma_m^{III}r_{BH}\}} \tag{37}$$

Model-5 [16–18]:

$$\begin{vmatrix}P_{g-1}&Q_{g-1,g}&Q_{g-1,g+1}\\Q_{g,g-1}&P_g&Q_{g,g+1}\\Q_{g+1,g-1}&Q_{g+1,g}&P_{g+1}\end{vmatrix}=0 \tag{38}$$

where

$$\begin{aligned}P_{v'}=&\left(J_{v'}'\{\gamma^{II}r_V\}-\frac{J_{v'}'\{\gamma^{II}r_W\}}{Y_{v'}'\{\gamma^{II}r_W\}}Y_{v'}'\{\gamma^{II}r_V\}\right)\left(\frac{2\pi}{N}-\varphi\right)\\&-\frac{2\pi}{N}\frac{\gamma^{II}}{\gamma^I}\frac{J_{v'}'\{\gamma^I r_V\}}{J_{v'}\{\gamma^I r_V\}}\left(J_{v'}\{\gamma^{II}r_V\}-\frac{J_{v'}'\{\gamma^{II}r_W\}}{Y_{v'}'\{\gamma^{II}r_W\}}Y_{v'}\{\gamma^{II}r_V\}\right)\end{aligned} \tag{39}$$

$$Q_{v',v}=\left(J_v'\{\gamma^{II}r_V\}-\frac{J_v'\{\gamma^{II}r_W\}}{Y_v'\{\gamma^{II}r_W\}}Y_v'\{\gamma^{II}r_V\}\right)\frac{1-\exp j(v'-v)\varphi}{j(v'-v)} \tag{40}$$

Model-6 [19]:

The dispersion relation for model-6 (**Figure 7**) is same as that for model-3 (**Figure 4**) and is given by (34) through (35) with interpretation of radial propagation constant in dielectric filled region as $\gamma_m^{II} = \left(\varepsilon_r k^2 - \beta_m^2\right)^{1/2}$ [19].

Model-7 [20]:

$$\det\left|M_{nm} J_0\{\gamma_n^I r_{MD}\}\left[J_0'\{\gamma_m^{II} r_D\} + \xi Y_0'\{\gamma_m^{II} r_D\}\right] - J_0'\{\gamma_n^I r_D\}\left[J_0\{\gamma_m^{II} r_D\} + \xi Y_0\{\gamma_m^{II} r_D\}\right]\right| = 0 \tag{41}$$

$$\xi = \frac{\gamma_m^{III} J_0'\{\gamma_m^{II} r_{DD}\} Z_0\{\gamma_m^{III} r_{DD}\} - \gamma_m^{II} J_0\{\gamma_m^{II} r_{DD}\} Z_0'\{\gamma_m^{III} r_{DD}\}}{\gamma_m^{II} Y_0\{\gamma_m^{II} r_{DD}\} Z_0'\{\gamma_m^{III} r_{DD}\} - \gamma_m^{III} Y_0'\{\gamma_m^{II} r_{DD}\} Z_0\{\gamma_m^{III} r_{DD}\}} \tag{42}$$

Model-8 [21]:

The dispersion relation for model-8 (**Figure 9**) is same as that for model-5 (**Figure 6**) and is given by (38) through (39) and (40) with interpretation of radial propagation constant in dielectric filled region as $\gamma^{II} = \left(\varepsilon_r k^2 - \beta^2\right)^{1/2}$ [21].

## 5. Dispersion characteristics

One may clearly observe that the shape of dispersion characteristics of the model-1 (**Figure 2**) and model-2 (**Figure 3**) change with change in relative permittivity of the dielectric material (**Figures 10** and **11**). The cutoff frequency decreases with increase of the relative permittivity of the dielectric material. The increase of relative permittivity of the dielectric material depresses the dispersion characteristics of the model-1 and model-2 and more at higher value of phase propagation constant. The analytical dispersion characteristics are found within 3% of that obtained using HFSS (**Figures 10** and **11**).

Periodic loading a circular waveguide by the metal annular discs (model-3) brings out alternate pass and stop bands with their respective higher and lower

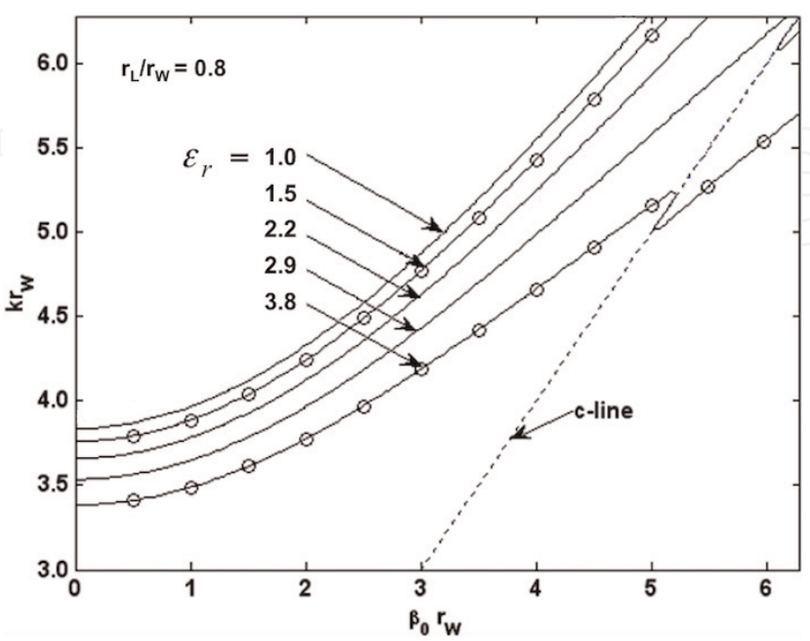


**Figure 10.**
*$TE_{01}$-mode dispersion characteristics of circular waveguide with dielectric lining on metal wall taking $\varepsilon_r$ as the parameter. The characteristics with $\varepsilon_r = 1$ (special case) represents the dispersion characteristics of conventional circular waveguide. Circles represent results obtained using HFSS.*

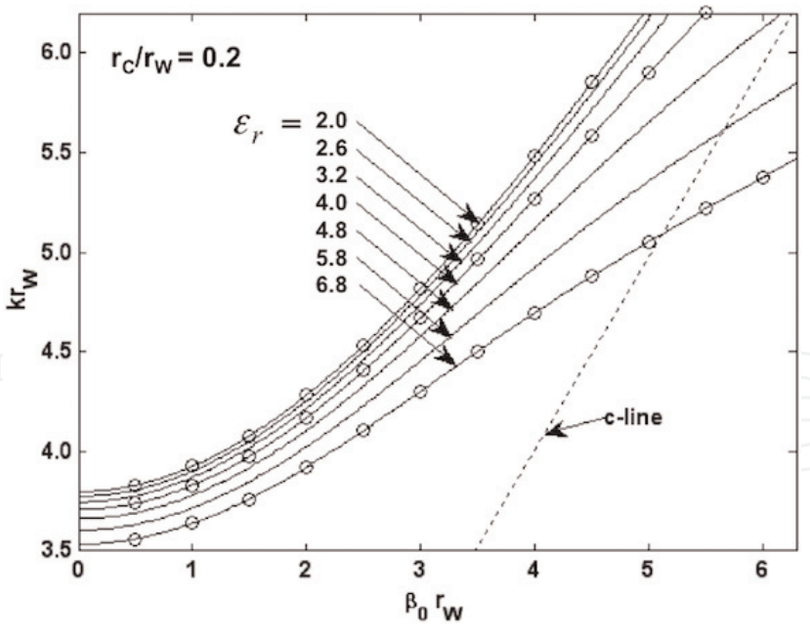


**Figure 11.**
*$TE_{01}$-mode dispersion characteristics of circular waveguide with coaxial dielectric rod and taking $\varepsilon_r$ as the parameter. Circles represent results obtained using HFSS.*

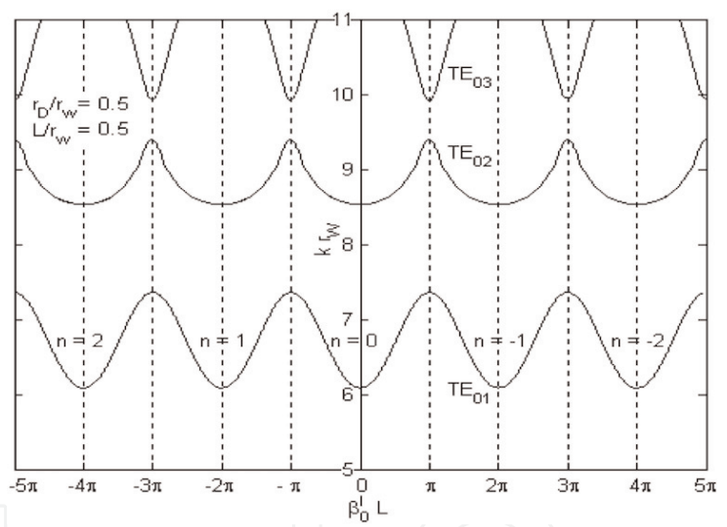


**Figure 12.**
*Pass and stop band characteristics of the infinitesimally thin metal disc-loaded circular waveguide (including higher order harmonics $n = 0, \pm 1, \pm 2, \pm 3, \pm 4, \pm 5$; $m = 1, 2, 3, 4, 5, 6, 7, 8, 9, 10, 11$) [9, 10].*

cutoff frequencies [1–3, 5, 9]. The dispersion characteristics taking horizontal axis as normalized phase propagation constant become periodic with the periodicity of $\beta_0^I L = 2\pi$ for a given mode ($TE_{01}$, $TE_{02}$ and $TE_{03}$). The normalized passband ($kr_W$ scale) for the $TE_{02}$ mode is narrower than that of the $TE_{01}$ mode. Similarly, the normalized stopband above the $TE_{02}$ mode is narrower than that above the $TE_{01}$ mode (**Figure 12**). The RF group velocity (slopes of dispersion plot) is positive (fundamental forward wave mode, $n$ = 0) for the TE01 or $TE_{02}$ mode, it is negative (fundamental backward wave mode) for the $TE_{03}$ mode (**Figure 12**). The dependencies of the structure dispersion characteristics, for typical mode $TE_{01}$, on the disc-hole radius (**Figure 13**), the structure periodicity (**Figure 14**) and the finite disc thickness (**Figure 15**) are studied. Further, with the increase of either of the parameters, namely, the disc-hole radius and the structure periodicity, the lower and upper edge frequencies of the passband of the dispersion characteristics both decrease, though not equally. This lead to decrease or increase of the passband

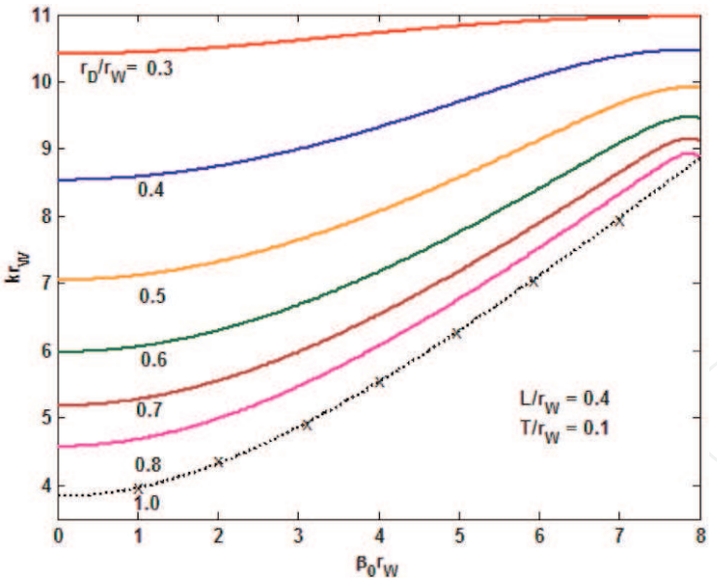


**Figure 13.**
*$TE_{01}$-mode dispersion characteristics of the conventional disc-loaded circular waveguide (solid curve) taking the disc-hole radius as the parameter. The broken curve with crosses refers to a smooth-wall circular waveguide [2, 5, 11].*

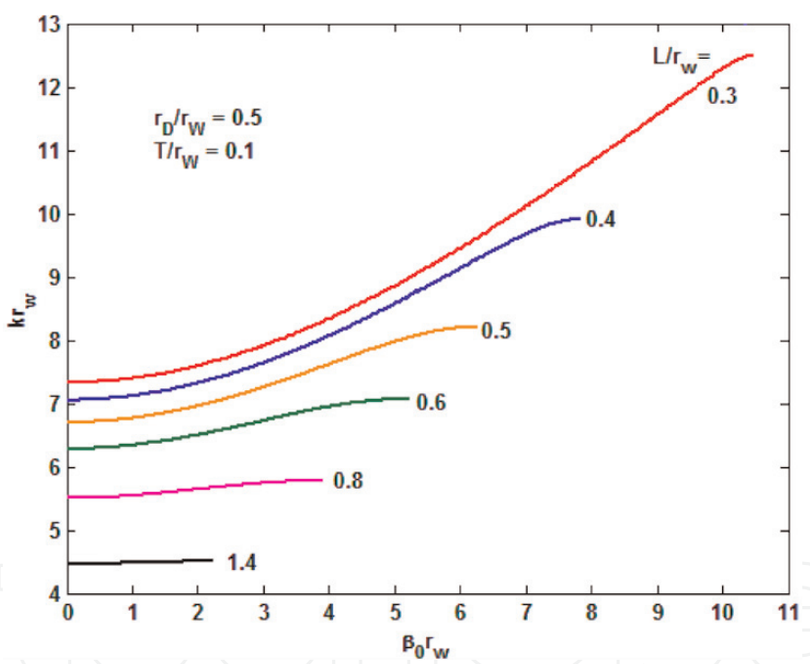


**Figure 14.**
*$TE_{01}$-mode dispersion characteristics of the conventional disc-loaded circular waveguide (solid curve) taking the structure periodicity as the parameter [2, 5, 11].*

according as the disc-hole radius decreases or the structure periodicity decreases, with the shift of the mid-band frequency of the passband to a higher value for the decrease of both the parameters (**Figures 13** and **14**) [2, 5, 11].

Although the disc-hole radius and the structure periodicity tailor the dispersion characteristics, the later one found to be more effective that the former one for widening the frequency range of the straight-line section of the characteristics. Reducing the structure periodicity can increase the frequency range of the straight-line section, however it accompanies with shift in waveguide cutoff (**Figure 14**). This wider straight-line section of the dispersion characteristics may be utilized for wideband coalescence with cyclotron wave (beam mode line) to result a wideband performance of a gyro-TWT. Thus, reducing the structure periodicity (**Figure 14**)

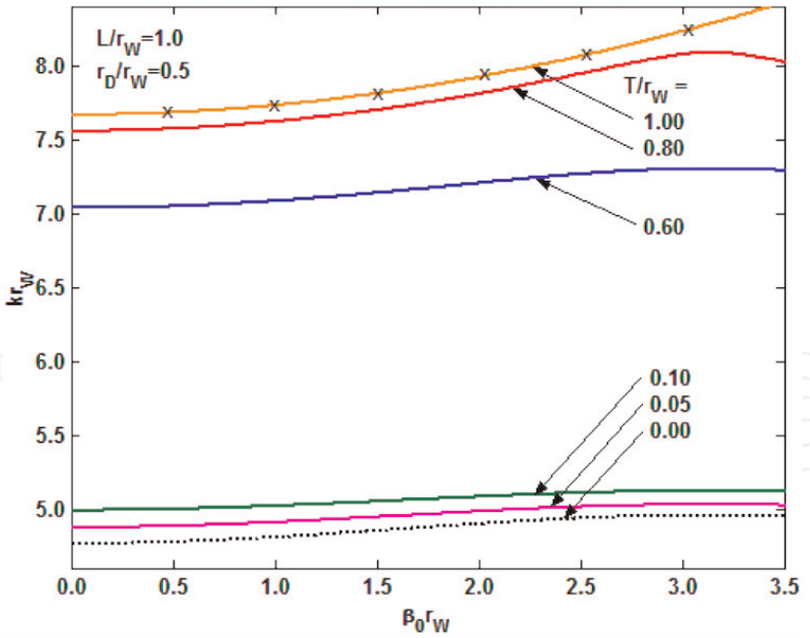


**Figure 15.**
*$TE_{01}$-mode dispersion characteristics of the conventional disc-loaded circular waveguide taking the disc thickness as the parameter. The broken curve refers to the infinitesimally thin metal disc-loaded circular waveguide [2, 5, 11].*

and increasing the disc-hole radius (**Figure 13**) may widen the device bandwidth. However, such broadbanding of coalescence is accompanied by the reduction of the bandwidth of the passband of the structure as well (**Figures 13** and **14**) [2, 5, 11]. The decrease of the disc thickness decreases both the lower and upper edge frequencies of the passband such that the passband first decreases, attains a minima and then increases; and the mid-band frequency of the passband as well as the start frequency of the straight-line section of the dispersion characteristics reduces (**Figure 15**). The shape of the dispersion characteristics depends on the disc thickness, though not as much as it does on the disc-hole radius or the structure periodicity (**Figures 13-15**) [2, 5, 11].

Similar to the conventional disc-loaded circular waveguide (model-3), both the hole-radii (bigger and smaller) of the interwoven-disc-loaded circular (model-4, **Figure 5**) waveguide tailor the dispersion characteristics. The lower- and the upper-cutoff frequencies decrease with increase in hole-radii, such that the passband increases and decreases with decrease of bigger and smaller hole-radii, respectively (**Figures 16** and **17**). Similar to the conventional disc-loaded circular waveguide (model-3), the structure periodicity of the interwoven-disc-loaded circular waveguide is the most effective for the increasing the passband and tailoring the dispersion characteristics (**Figure 18**). Neither, the extent of passband changes nor dispersion tailors with variation of disc-thickness of bigger-hole-disc, however, the mid frequency of the passband shifts to higher frequency with increase of disc-thickness of bigger-hole-disc (**Figure 19**). This nature may be used for shifting the operation band in the passive components or in order to optimizing the beam-wave interaction in designing a gyro-TWT with the interwoven-disc-loaded circular waveguide. In addition to tailoring the dispersion characteristics, required for designing a broadband gyro-TWT, the model-4 shows an interesting characteristic. The passband increases with increase as well as with decrease of disc-thickness of smaller- hole-disc with reference to that of bigger-hole-disc, however, the shift of the passband occur towards higher and lower frequency side, respectively, with increase and decrease of disc thickness of smaller-hole-disc with reference to that of bigger-hole-disc (**Figure 20**). Thus, the structure periodicity (**Figure 18**) and the

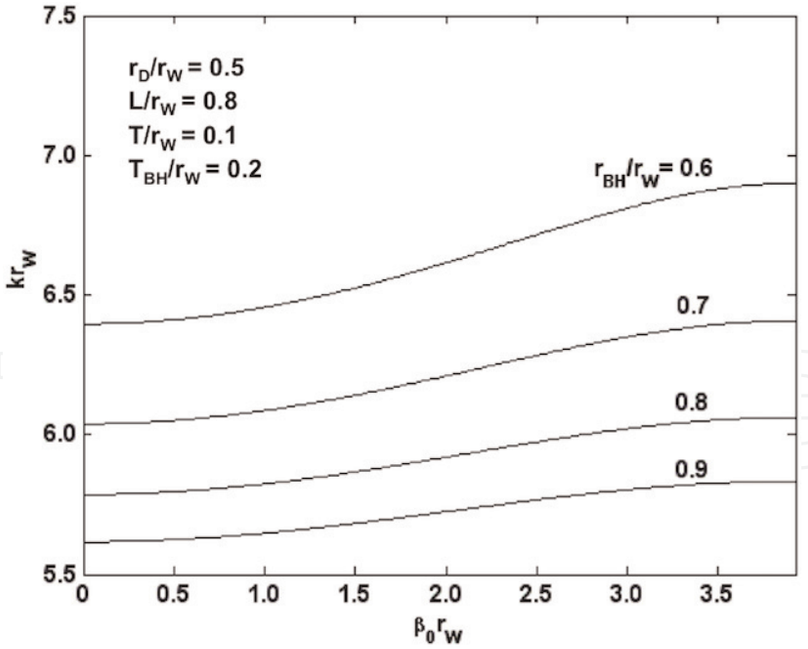


**Figure 16.**
*$TE_{01}$-mode dispersion characteristics of the interwoven-disc-loaded circular waveguide taking the bigger disc-hole-radius as the parameter [9, 14, 15].*

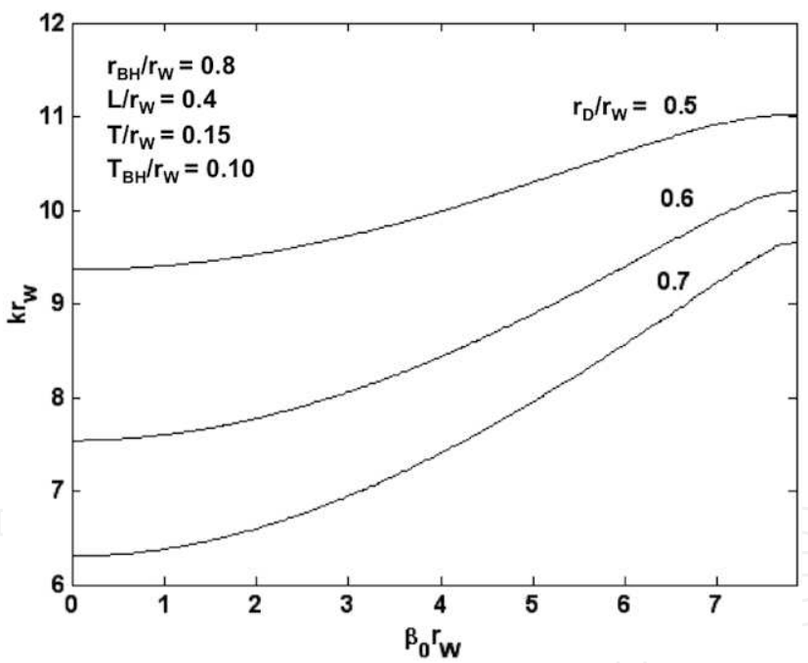


**Figure 17.**
*$TE_{01}$-mode dispersion characteristics of the interwoven-disc-loaded circular waveguide taking the smaller disc-hole-radius as the parameter [9, 14, 15].*

disc-thickness (**Figure 19**) of bigger-hole-disc of the interwoven-disc-loaded circular waveguide are, respectively, the most and the least sensitive parameter for controlling the passband as well as shape of the dispersion characteristics [14, 15].

Axial metal vane loading to a smooth-wall circular waveguide (model-5, **Figure 6**) forms an azimuthally periodic structure, which does not shape its dispersion characteristics, however the insertion of the metal vanes in to the circular waveguide shifts the waveguide cutoff frequency to a higher value [16–18] (**Figures 21–23**). Specifically, the increase of either of the vane angle (**Figure 22**) and the number of metal vanes (**Figure 23**) and the decrease of vane-inner-tip

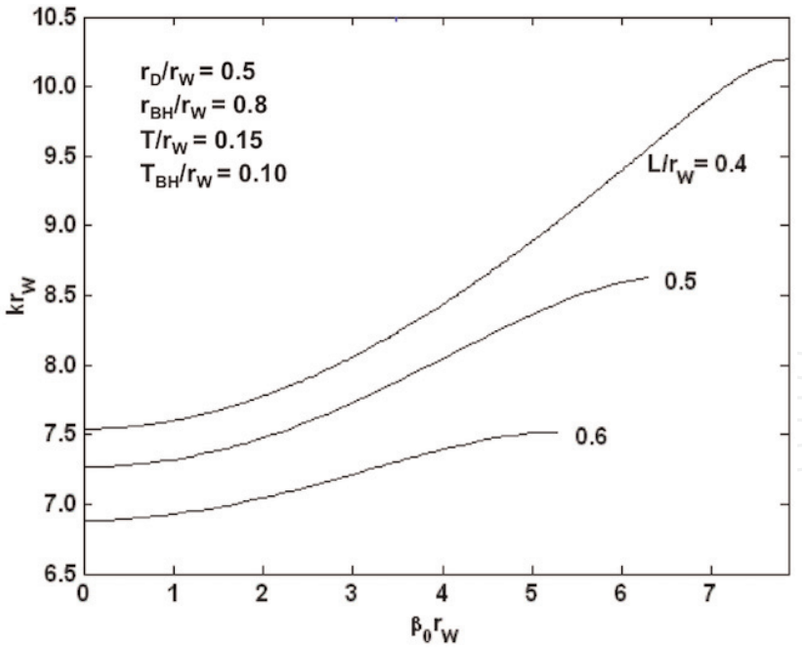


**Figure 18.**
*$TE_{01}$-mode dispersion characteristics of the interwoven-disc-loaded circular waveguide taking the structure periodicity as the parameter [9, 14, 15].*

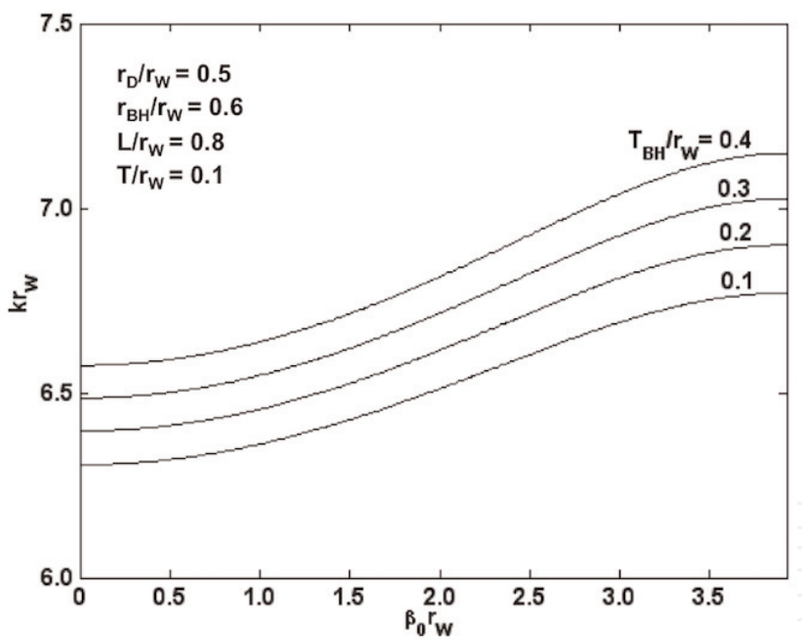


**Figure 19.**
*$TE_{01}$-mode dispersion characteristics of the interwoven-disc-loaded circular waveguide taking the disc-thickness of bigger-hole-disc as the parameter [9, 14, 15].*

radius (**Figure 21**) increases the waveguide cutoff frequency, and none of the parameters tailors the dispersion characteristics.

For the model-6, the variation of relative permittivity of the dielectric discs changes the lower and upper cutoff frequencies of the passband (**Figure 24**). Two lowest order azimuthally symmetric ($TE_{01}$ and $TE_{02}$) modes are typically considered to study the performance of this model. With the increase of relative permittivity, the passband continuously decreases for the $TE_{01}$ mode, and first decreases and then increases for the $TE_{02}$ mode (**Figure 24**). Also, the variation in relative permittivity shapes of the dispersion characteristics of the structure, for both the

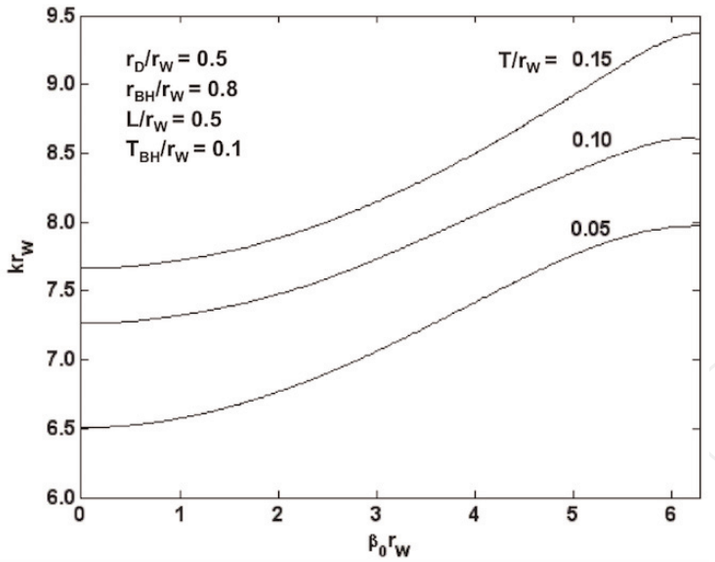


**Figure 20.**
*$TE_{01}$-mode dispersion characteristics of the interwoven-disc-loaded circular waveguide taking the disc thickness of smaller-hole-disc as the parameter [9, 14, 15].*

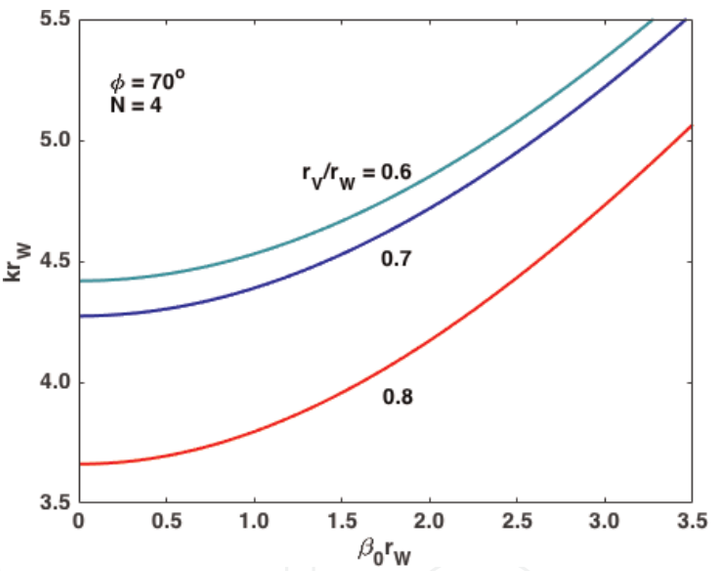


**Figure 21.**
*$TE_{01}$-mode dispersion characteristics of the metal-vane-loaded circular waveguide taking the vane-inner-tip radius as the parameter [16–18].*

modes $TE_{01}$ and $TE_{02}$, however more significantly for the latter mode (**Figure 24**). The $TE_{01}$ mode of the structure.

Exhibits fundamental forward wave (positive) dispersion characteristics irrespective of the value of relative permittivity (**Figure 24(a)**), however, the $TE_{02}$ mode exhibits fundamental forward (positive) and backward (negative) wave dispersion characteristics, respectively, at higher and lower values of relative permittivity. This suggests that an appropriate selection of the value of relative permittivity in this structure would yield a straightened $TE_{02}$ mode $\omega - \beta$ dispersion characteristics near low value of phase propagation constant for wideband coalescence with the beam-mode dispersion line and consequent wideband gyro-TWT performance (**Figure 24(b)**). Thus the introduction of the dielectric discs between metal discs in the a conventional metal disc-loaded waveguide, with lower values of relative permittivity for the $TE_{01}$ mode and with higher values of relative permittivity for the $TE_{02}$ mode enhances the frequency range of the straight line portion of

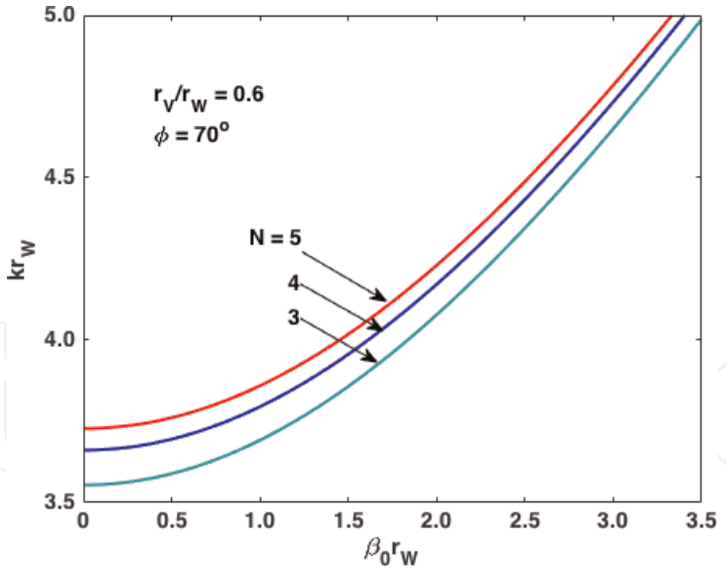


**Figure 22.**
*$TE_{01}$-mode dispersion characteristics of the metal-vane-loaded circular waveguide taking the vane angle as the parameter [16–18].*

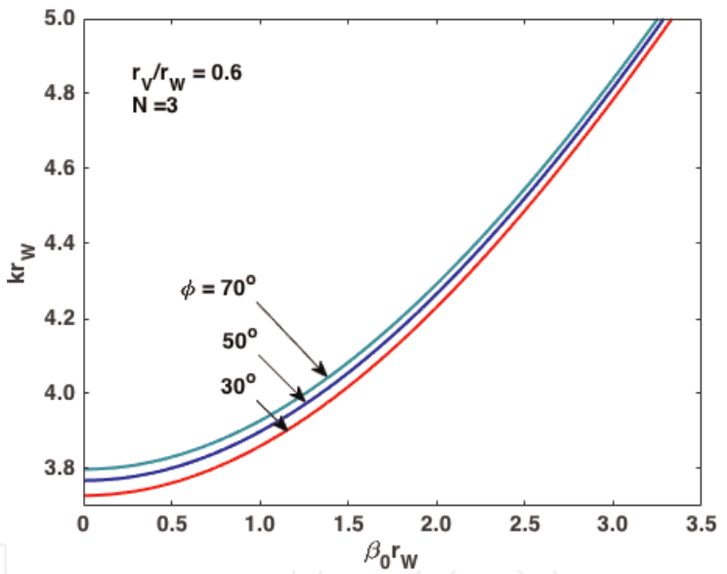


**Figure 23.**
*$TE_{01}$-mode dispersion characteristics of the metal-vane-loaded circular waveguide taking the number of metal vanes as the parameter [16–18].*

the $\omega - \beta$ dispersion characteristics, desired for wideband gyro-TWT performance (**Figure 25**) [19].

The lower and upper cutoff frequencies of the passband vary with thickness of dielectric disc $(L - T)/r_W$ taking structure periodicity constant such that the passband decreases with an increase in thickness of dielectric disc for both the $TE_{01}$ and $TE_{02}$ modes. The thickness of dielectric disc tailors the dispersion characteristics, however, more for the $TE_{02}$ than for the $TE_{01}$ mode, and the control is more prominent for thinner dielectric disc (**Figure 26**) [19]. The less effective parameters, the disc-hole radius, in tailoring the dispersion characteristics of a conventional disc-loaded waveguide [2, 5, 9–13], effectively controls the shape of the characteristics after introducing the dielectric discs between the metal discs, while, the control is more for the $TE_{02}$ (**Figure 27(b)**) than for the $TE_{01}$ (**Figure 27(a)**) mode, however the characteristics is little irregular for higher disc-hole radius

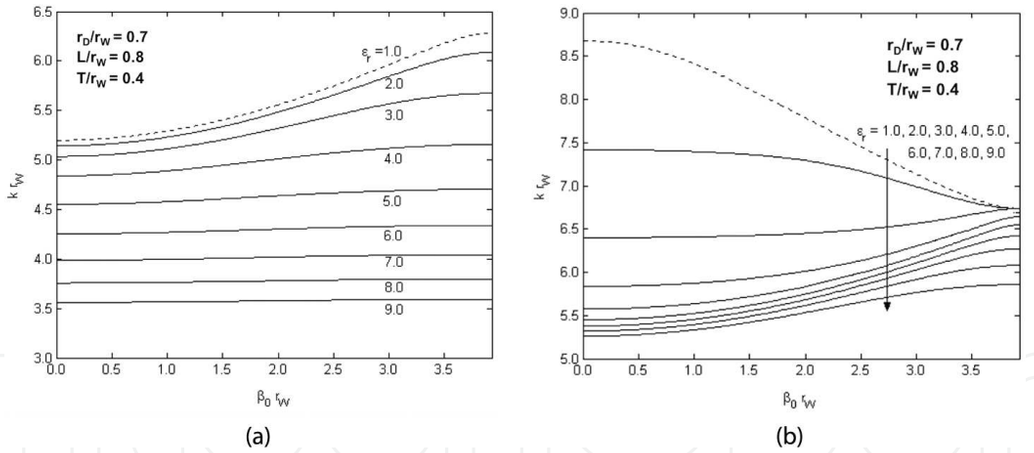


**Figure 24.**
*$TE_{01}$ (a) and $TE_{02}$ (b) mode dispersion characteristics of a circular waveguide loaded with alternate dielectric and metal annular discs (model-6) taking relative permittivity as the parameter. The broken curves refer to a conventional metal disc-loaded circular waveguide [19].*

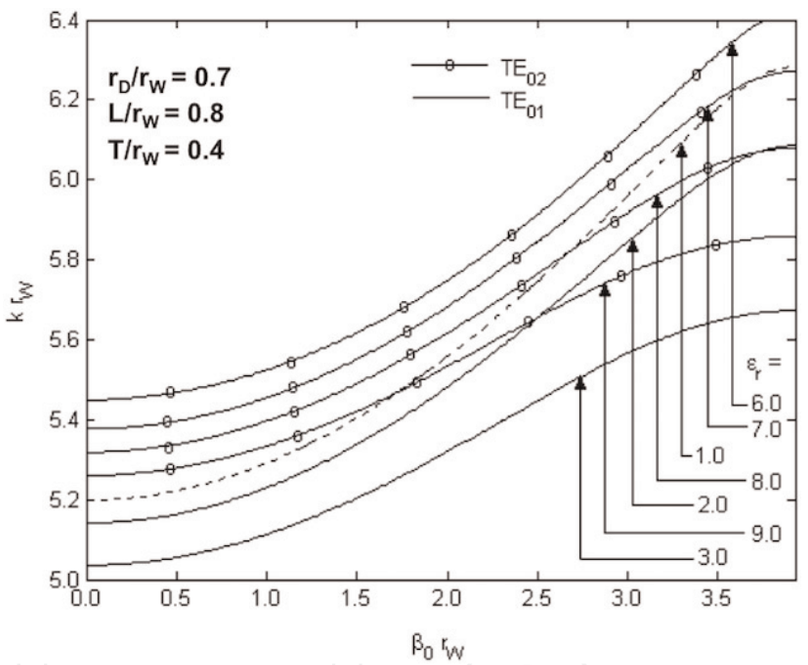


**Figure 25.**
*Dispersion characteristics of a circular waveguide loaded with alternate dielectric and metal annular discs (model-6) for the selected dielectric disc relative permittivity values for the sake of comparison between the modes $TE_{01}$ and $TE_{02}$ with respect to the control of the shape of the dispersion characteristics. The broken curves referring to a conventional metal disc-loaded circular waveguide [19].*

(**Figure 27**) [19]. Similar to a conventional all-metal disc-loaded waveguide (model-4), the structure periodicity is the most effective parameter for tailoring the dispersion characteristics of the structure with dielectric discs between the metal discs (model-6), for the $TE_{01}$ and $TE_{02}$ modes, more for the latter. The control of the structure periodicity in straightening the dispersion characteristics, as required for the desired wideband gyro-TWT performance, is enhanced by introducing the dielectric discs in the conventional disc-loaded waveguide, though not enhancing the frequency range of the straight line portion of the dispersion characteristics (**Figure 28**). In this model, a serious care is required while selecting the dielectric material because a heavily dielectric-loaded structure depresses the dispersion characteristics to the slow-wave region (below the velocity of light line in $\omega - \beta$ characteristics).

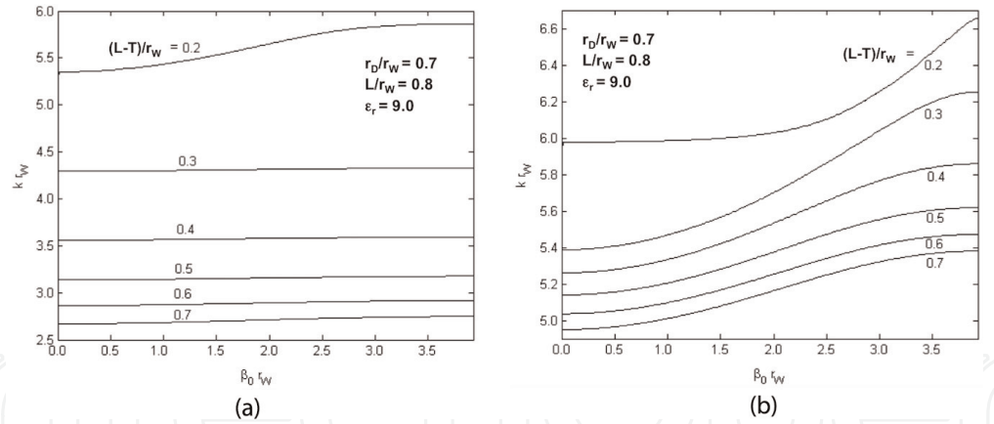


**Figure 26.**
*$TE_{01}$ (a) and $TE_{02}$ (b) mode dispersion characteristics of a circular waveguide loaded with alternate dielectric and metal annular discs (model-6) taking dielectric disc thickness as the parameter for a constant structure periodicity [19].*

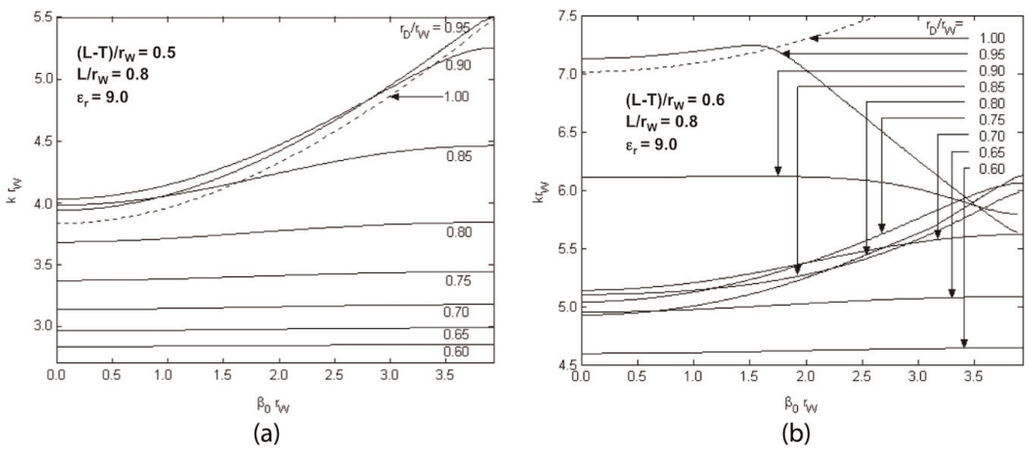


**Figure 27.**
*$TE_{01}$ (a) and $TE_{02}$ (b) mode dispersion characteristics of a circular waveguide loaded with alternate dielectric and metal annular discs (model-6) taking the disc-hole radius as the parameter. The broken curves refer to the special case of a conventional smooth wall circular waveguide [19].*

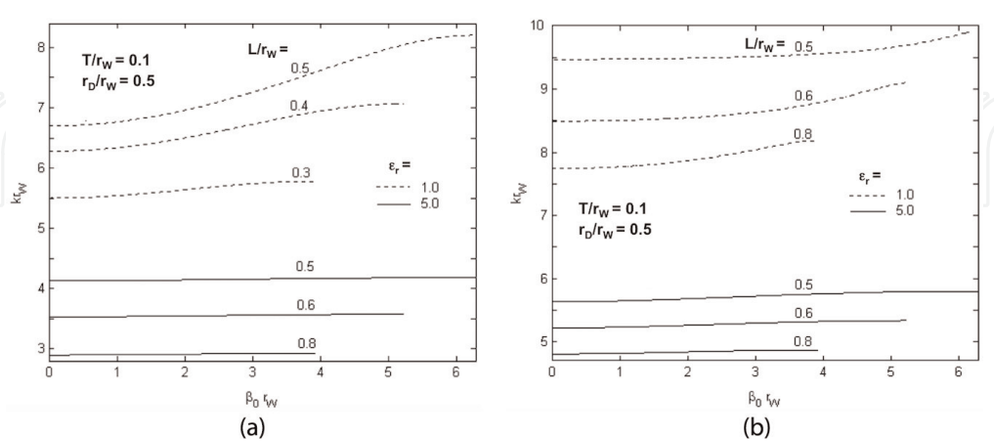


**Figure 28.**
*$TE_{01}$ (a) and $TE_{02}$ (b) mode dispersion characteristics of a circular waveguide loaded with alternate dielectric and metal annular discs (model-6) taking structure periodicity as the parameter. The broken curves refer to a conventional metal disc-loaded circular waveguide [19].*

We choose first three lowest order azimuthally symmetric modes in the composite (dielectric and metal) loaded structures for exploring the effect of structure parameter on dispersion characteristics while we chose only the lowest order

azimuthally symmetric mode in all-metal variants of the axially periodic structure. The increase of the relative permittivity of the dielectric discs in model-7 reduces the lower and upper cutoff frequencies, however not equally therefore shortens the passband for the $TE_{01}$ mode with shift of the mid-frequency of the passband towards lower value (**Figure 29(a)**). With the increase of the relative permittivity of the dielectric discs, the lower and upper cutoff frequencies shift to lower value for the $TE_{01}$ and $TE_{02}$ modes. The quantitatively the shift in upper cutoff frequency is higher than that of lower cutoff frequency for the $TE_{01}$, which in turn shortens the passband (**Figure 29(a)**), however, the shift in lower and upper cutoff frequencies are almost equal for the $TE_{02}$ mode, effectively the passband does not change (**Figure 29(b)**). Interestingly for the $TE_{02}$ mode the introduction of dielectric discs converts the fundamental backward mode (the zero group velocity follows to take negative values then again zero and further positive) into fundamental forward mode (the zero group velocity follows to take positive values then again zero and further negative) (**Figure 29(b)**). Thus, introduction of dielectric discs into the conventional disc-loaded waveguide turns the negative dispersion into positive. In absence as well as in presence of the dielectric discs, the $TE_{03}$ mode dispersion characteristics of the disc-loaded waveguide represents the fundamental backward mode, in which the increase of the relative permittivity of the dielectric discs shifts the lower cutoff frequency more than that of upper cutoff frequency, and thus widens the passband for lower relative permittivity. For higher relative permittivity value the lower cutoff frequency remains unchanged and upper cutoff frequency shifts to lower value with the increase of the relative permittivity of the dielectric discs and shortens the passband (**Figure 29(c)**) [20, 21].

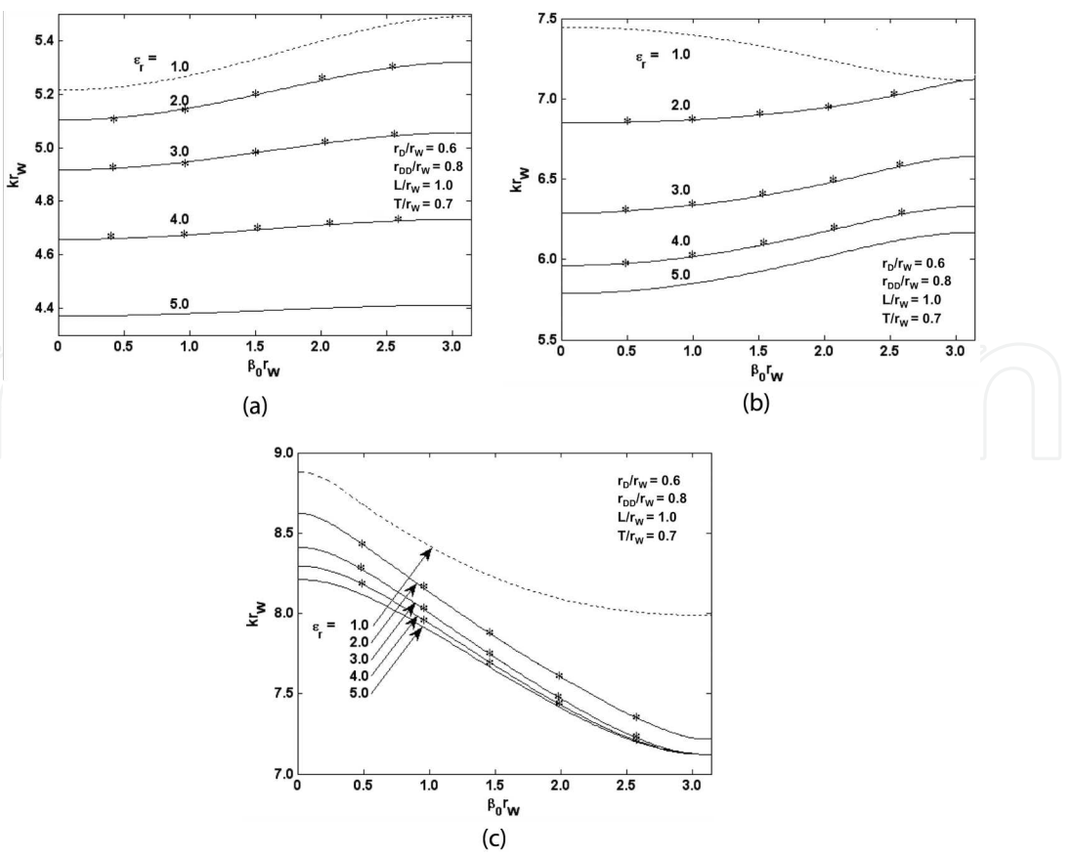


**Figure 29.**
*$TE_{01}$ (a), $TE_{02}$ (b) and $TE_{03}$ (c) mode dispersion characteristics of the alternate dielectric and metal disc-loaded circular waveguide taking relative permittivity of dielectric disc as the parameter [20, 21]. The broken curve refers to the conventional disc-loaded circular waveguide [2, 5, 9–13].*

The increase of dielectric disc radius in the model-7 taking constant metal disc radius shifts the lower and upper cutoff frequencies of the $TE_{01}$ mode up, and the passband increases due to lesser the shift in lower cutoff frequency (**Figure 30**). Similarly, the passband of the $TE_{02}$ mode increases with the increase of dielectric disc radius. Here, it is interesting to note that for the taken structure parameters ($r_D/r_W = 0.6$, $L/r_W = 1.0$, $T_{DD}/r_W = 0.3$ and $\varepsilon_r = 5.0$) the frequency shift is maximum for $r_{DD}/r_W$ equal to 0.8–0.9, and minimum for 0.7–0.8 (**Figure 30(b)**). For the lower and higher values of inner dielectric disc radius, the $TE_{03}$ mode dispersion characteristics of the model-7 are fundamental forward (positive) and backward (negative) modes respectively. Thus, there is a possibility of getting straight-line dispersion characteristics parallel to phase propagation constant axis, i.e., zero group velocity line (**Figure 30(c)**) [20, 21]. The increase of periodicity of the alternate dielectric and metal disc-loaded circular waveguide (model-7) reduces the passband and both the lower and upper cutoff frequencies with higher relative reduction in upper cutoff frequency than that of lower (**Figure 31**) for the chosen three azimuthally symmetric modes $TE_{01}$, $TE_{02}$ and $TE_{03}$. The $TE_{01}$ and $TE_{02}$ modes are fundamental forward and the $TE_{03}$ is fundamental backward [20, 21]. The change of dielectric disc thickness does not much tailor the dispersion characteristics and the passband (**Figure 32**), however, the decrease of the dielectric disc thickness or the increase of metal disc thickness shifts the passband to lower frequency side for the $TE_{01}$ and $TE_{02}$ modes (**Figure 31(a)** and **(b)**) and least change occur to the $TE_{03}$ mode. In very precise observation, the lower cutoff frequency of the $TE_{03}$ mode is insensitive and the upper cutoff frequency first decreases and then increases with decrease of dielectric disc thickness or with increase of metal disc thickness (**Figure 32**) [20, 21].

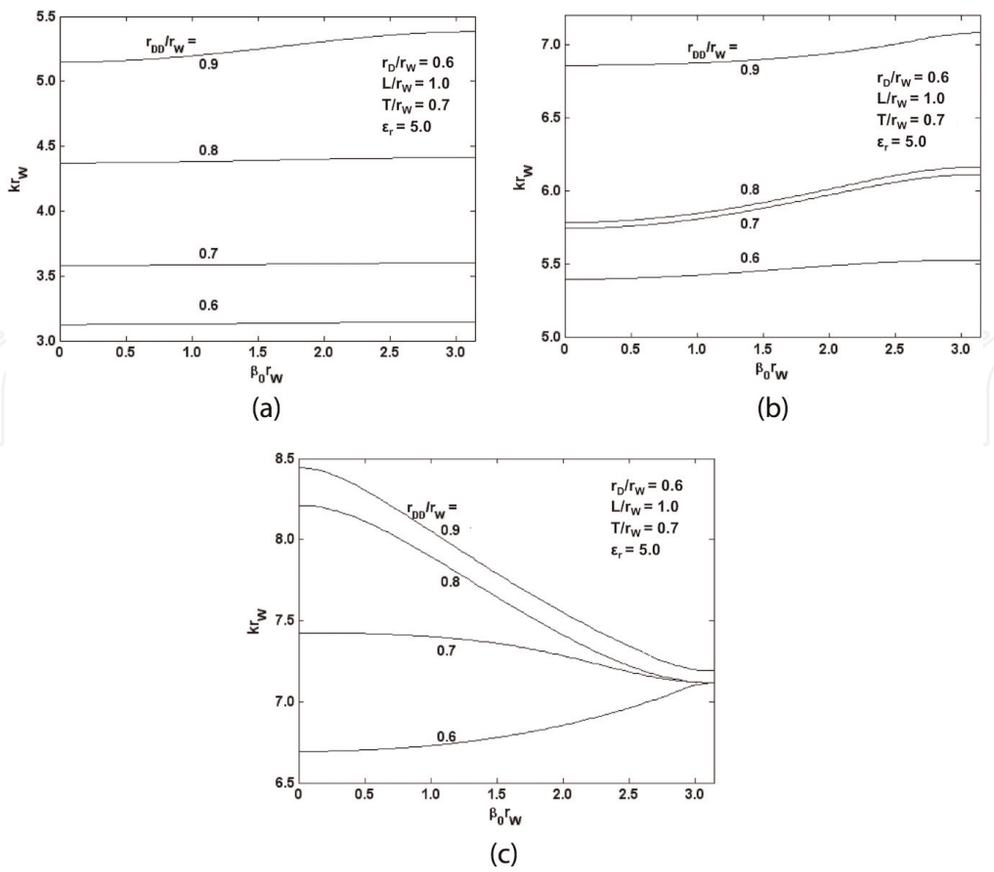


**Figure 30.**
*$TE_{01}$ (a), $TE_{02}$ (b) and $TE_{03}$ (c) mode dispersion characteristics of the alternate dielectric- and metal disc-loaded circular waveguide (model-7) taking inner radius of dielectric disc as the parameter [20, 21].*

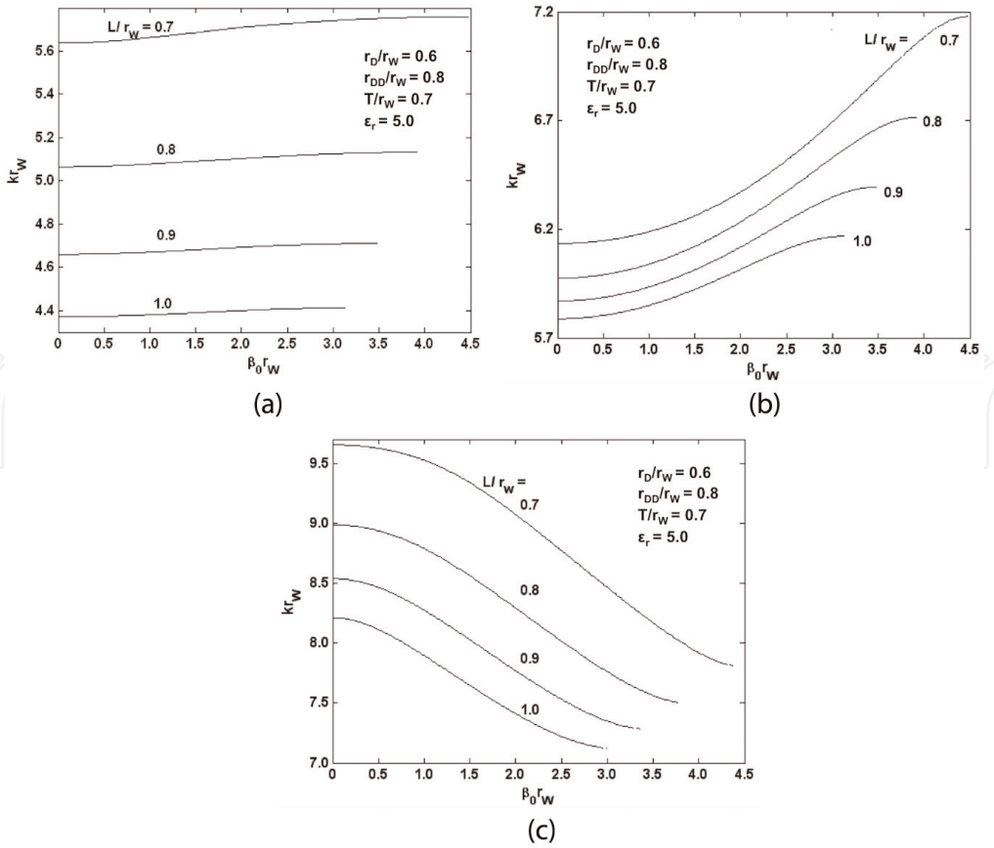


**Figure 31.**
*$TE_{01}$ (a), $TE_{02}$ (b) and $TE_{03}$ (c) mode dispersion characteristics of the alternate dielectric and metal disc-loaded circular waveguide (model-7) taking structure periodicity as the parameter [20, 21].*

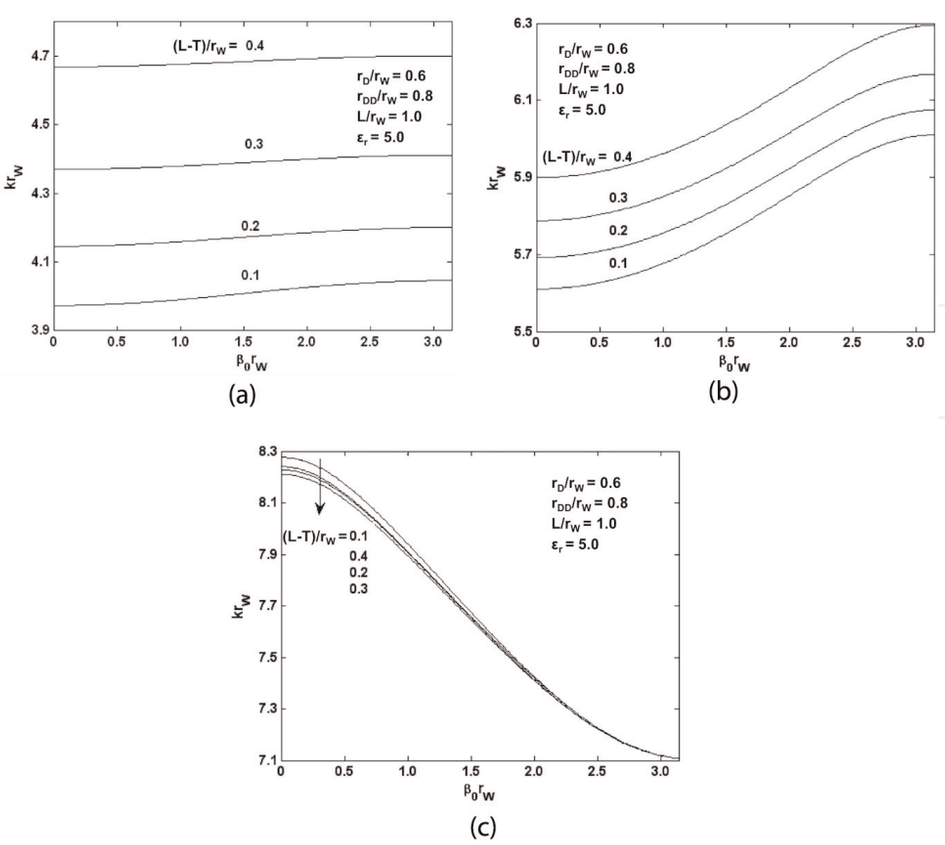


**Figure 32.**
*$TE_{01}$ (a), $TE_{02}$ (b) and $TE_{03}$ (c) mode dispersion characteristics of the alternate dielectric and metal disc-loaded circular waveguide (model-7) taking thickness of dielectric disc as the parameter [20, 21].*

Although the geometrical parameters do not tailor the dispersion characteristics of the only metal vane-loaded waveguide [16–18], however, it does for composite-loaded structure (model-8). The radial dimensions (**Figure 33**) are less sensitive in tailoring the dispersion characteristics of the dielectric and metal vanes than their angular dimensions (**Figure 34**), relative permittivity (**Figure 35**) and number of vanes (**Figure 36**). However, the waveguide cutoff (eigenvalue) of the structure depends on all these parameters (**Figures 33-36**). Thus, one may choose angular dimensions, relative permittivity and number of vanes for tailoring the dispersion characteristics and the radial parameter to control the waveguide cutoff frequency [21].

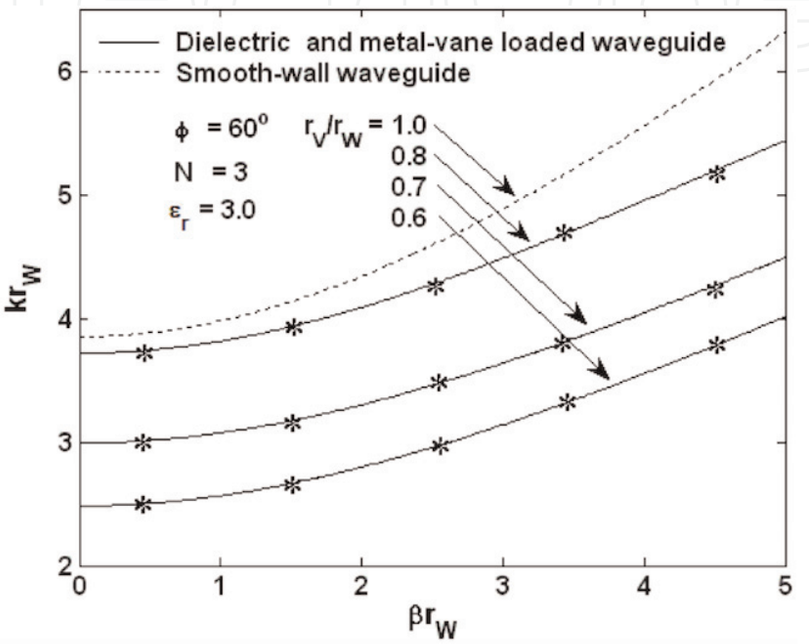


**Figure 33.**
*$TE_{01}$-mode dispersion characteristics of a circular waveguide loaded with composite alternate dielectric and metal vanes taking the vane inner-tip radius as the parameters. The broken curve refers to a smooth-wall waveguide (free from dielectric and metal vanes) and the star (*) marker refers representative points obtained using HFSS [21].*

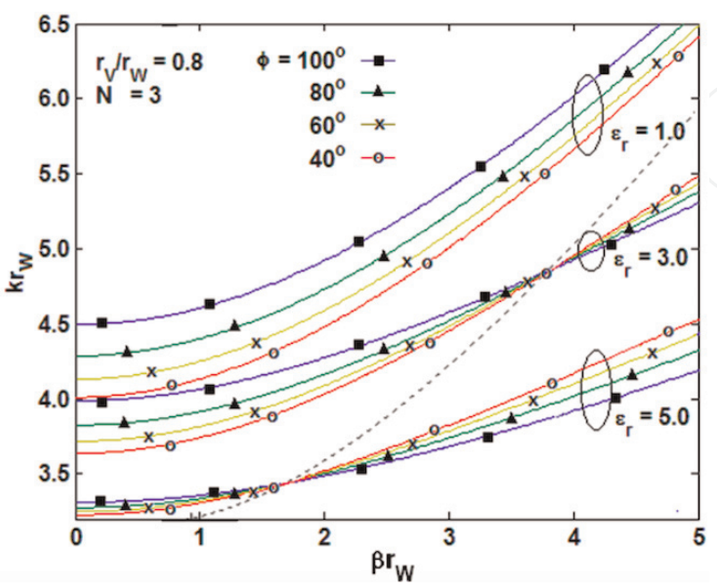


**Figure 34.**
*$TE_{01}$-mode dispersion characteristics of a circular waveguide loaded with dielectric and metal vanes taking metal vane angle as the parameter. The broken curve represents the locus of the crossover point, which is same as the dispersion characteristics of the smooth-wall circular waveguide of radius $r_V$ [21].*

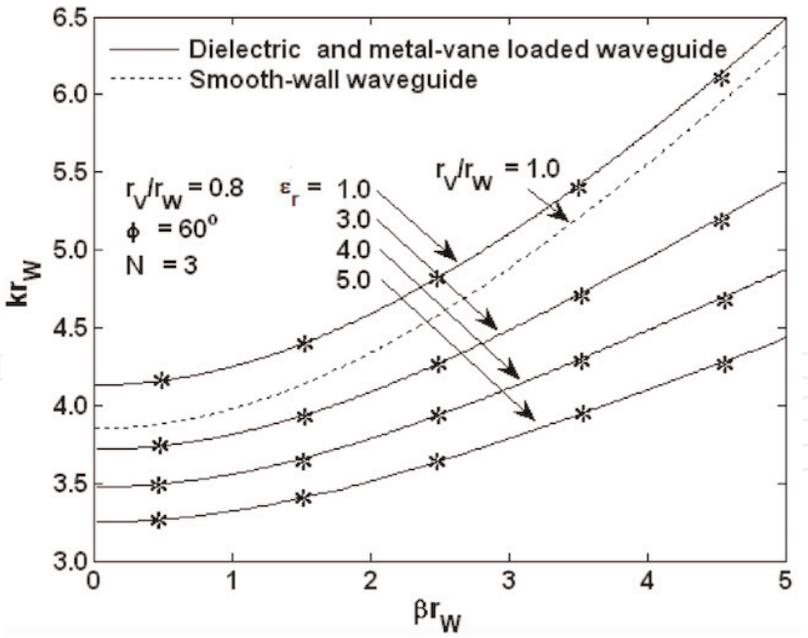


**Figure 35.**
*$TE_{01}$-mode dispersion characteristics of a circular waveguide loaded with composite alternate dielectric and metal vanes, taking the relative permittivity of dielectric vanes as the parameters, along with the corresponding characteristics of a smooth-wall waveguide (free from dielectric and metal vanes) (broken curve) and the typical representative points of the characteristics obtained by simulation (HFSS) (* (star) marker) [21]. $\varepsilon_r = 1$ represents the characteristics of a waveguide loaded with metal vanes alone (**Figure 6**) [16–18].*

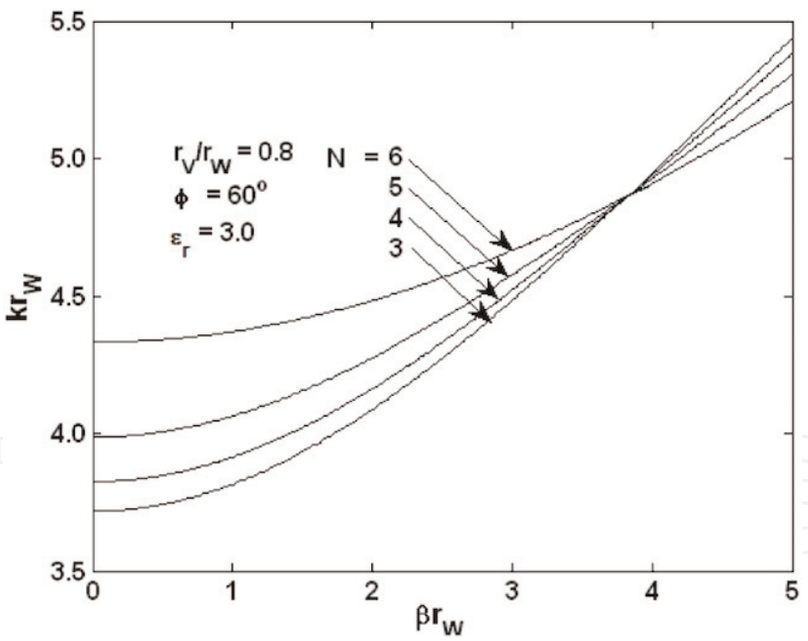


**Figure 36.**
*$TE_{01}$-mode dispersion characteristics of a circular waveguide loaded with dielectric and metal vanes taking number of vanes as the parameter [21].*

A crossover point in the dispersion characteristics appears with varying metal vane angle (**Figure 34**) or varying number of vanes (**Figure 36**). This crossover point sifts to another location for another value of relative permittivity. The locus of such crossover points for varying relative permittivity overlaps with the dispersion plot of a smooth-wall circular waveguide of radius equal to the vane tip radius (**Figure 34**). Below the crossover point, the increase of metal cross-section (either by increasing metal vane angle or by increasing number of vanes) in the cross-section of the waveguide elevates and that of dielectric depresses the dispersion

characteristics, and vice versa above the crossover point. This clearly represents the behavior of model-8 as a smooth-wall waveguide of wall radius equal to the vane tip radius at the crossover point and change of metal cross-section (either by changing metal vane angle or by changing number of vanes) in the cross-section of the waveguide affects the dispersion characteristics away from the crossover (**Figures 34** and **36**) [21].

## 6. Conclusion

The waveguide is inherently a high pass filter with a lower cut-off frequency, a signal of above this frequency will be allowed to propagate or travel through the waveguide. Different kind of loading, such as metal and/or dielectric, has been suggested in the published literature for altering the propagation (dispersion) characteristics. In the present chapter a number of loaded structures are studied with circular cross-sections. All the structure parameters are varied to explore the sensitivity over the dispersion characteristics. In general, the axial periodicity results in periodic dispersion characteristics with a lower and an upper cut-off frequency, which makes the guiding structure a bandpass structure. However, such a characteristic is not reported in literature for the azimuthal periodic structures. The bandpass characteristic arises due to the shaping of the dispersion characteristics. Therefore, the dispersion shaping is only possible with axial periodicity and not with the azimuthal periodicity in all metal structure. However, the azimuthal periodicity in all metal waveguide structure shifts the cut-off frequency over the frequency scale. The dispersion characteristics of various loaded structures have been explored. It has been the interest to study the change in the lower and upper cut-off frequencies and in the passband. The sensitivity of the structure (geometry) parameters on the lower and upper cut-off frequencies and the extent of passband are also included. In case of conventional disc-loaded structure, the periodicity is found to be the most sensitive parameter for dispersion shaping and the disc-hole radius is the most sensitive parameter for shifting the dispersion characteristics over the frequency axis. In interwoven-disc-loaded circular waveguide, the structure periodicity and the disc-thickness of bigger-hole-disc are, respectively, the most and the least sensitive parameter for controlling the passband as well as shape of the dispersion characteristics. Insertion of metal vanes to a circular waveguide does not shape the dispersion characteristics but increases the waveguide cutoff frequency. On the other hand, introduction of dielectric discs into the conventional disc-loaded waveguide turns the negative dispersion into positive. In case of composite vane-loaded structure, the angular dimensions, relative permittivity and number of vanes tailor the dispersion characteristics and the radial parameter controls the waveguide cutoff frequency.

*DOI: http://dx.doi.org/10.5772/intechopen.82124*





## Author details

Vishal Kesari
Microwave Tube Research and Development Centre, Defence Research and Development Organisation, Bangalore, India

*Address all correspondence to: vishal_kesari@rediffmail.com

## References

[1] Watkins DA. Topics in Electromagnetic Theory. New York: John Wiley; 1958

[2] Kesari V, Basu BN. High Power Microwave Tubes: Basics and Trends. San Rafael (CA)/Bristol: IOP Concise Physics, Morgan & Claypool Publishers/ IOP Publishing; 2018

[3] Collin RE. Foundations for Microwave Engineering. 2nd ed. USA: Wiley-IEEE Press; 2001

[4] Basu BN. Electromagnetic Theory and Applications in Beam-Wave Electronics. Singapore: World Scientific; 1996

[5] Kesari V. Analysis of Disc-Loaded Circular Waveguides for Wideband Gyro-TWTs. Koln: Lambert Academic Publishing AG & Co.; 2009

[6] Fliflet AW. Linear and nonlinear theory of the Doppler-shifted cyclotron resonance maser based on TE and TM waveguide modes. International Journal of Electronics. 1986;**61**(6):1049-1080

[7] Rao SJ, Jain PK, Basu BN. Broadbanding of gyro-TWT by dispersion shaping through dielectric loading. IEEE Transactions on Electron Devices. 1996;**43**:2290-2299

[8] Choe JY, Uhm HS. Theory of gyrotron amplifiers in disc or helix-loaded waveguides. International Journal of Electronics. 1982;**53**:729-741

[9] Kesari V, Basu BN. Analysis of some periodic structures of microwave tubes: Part II: Analysis of disc-loaded fast-wave structures of gyro-traveling-wave tubes. Journal of Electromagnetic Waves and Applications. 2018;**32**(4): 1-36

[10] Kesari V, Jain PK, Basu BN. Approaches to the analysis of a disc loaded cylindrical waveguide for potential application in wideband gyro-TWTs. IEEE Transactions on Plasma Science. 2004;**32**(5):2144-2151

[11] Kesari V, Jain PK, Basu BN. Analysis of a circular waveguide loaded with thick annular metal discs for wideband gyro-TWTs. IEEE Transactions on Plasma Science. 2005;**33**(4):1358-1365

[12] Kesari V, Jain PK, Basu BN. Analysis of a disc-loaded circular waveguide for interaction impedance of a gyrotron amplifier. International Journal of Infrared and Millimeter Waves. 2005; **26**(8):1093-1110

[13] Kesari V, Jain PK, Basu BN. Modal analysis of a corrugated circular waveguide for wideband potential in gyro-devices. International Journal of Microwave and Optical Technology. 2007;**2**(2):147-152

[14] Kesari V, Keshari JP. Interwoven-disc-loaded circular waveguide for a wideband gyro-traveling-wave tube. IEEE Transaction on Plasma Science. 2013;**41**(3):456-460

[15] Kesari V, Keshari JP. Propagation characteristics of a variant of disc-loaded circular waveguide. Progress in Electromagnetic Research. 2012;**26**: 23-37

[16] Singh G, Ravi Chandra SMS, Bhaskar PV, Jain PK, Basu BN. Analysis of dispersion and interaction impedance characteristics of an azimuthally-periodic vane-loaded cylindrical waveguide for a gyro-TWT. International Journal of Electronics. 1999;**86**:1463-1479

[17] Agrawal M, Singh G, Jain PK, Basu BN. Analysis of a tapered vane loaded broad-band gyro-TWT. IEEE Transactions on Plasma Science. 2001; **29**:439-444

[18] Shrivastava UA. Small-signal theories of harmonic gyrotron and peniotron amplifiers and oscillators [thesis]. Utah: University of Utah; 1985

[19] Kesari V, Jain PK, Basu BN. Modeling of axially periodic circular waveguide with combined dielectric and metal loading. Journal of Physics D: Applied Physics. 2005;**38**:3523-3529

[20] Kesari V, Keshari JP. Analysis of a circular waveguide loaded with dielectric and metal discs. Progress in Electromagnetic Research. 2011;**111**: 253-269

[21] Kesari V. Analysis of alternate dielectric and metal vane loaded circular waveguide for a wideband gyro-TWT. IEEE Transactions on Electron Devices. 2014;**61**(3):915-920